

Spatial distribution of scattering loss and intrinsic absorption of short-period *S* waves in the lithosphere of Japan on the basis of the Multiple Lapse Time Window Analysis of Hi-net data

Q1

Eduard Carcolé* and Haruo Sato

Department of Geophysics, Graduate School of Science, Tohoku University. Aramaki-Aza-Aoba 6-3, Aoba-ku, Sendai-shi. Miyagi-ken 980-8578, Japan.
E-mail: eduard@zisin.geophys.tohoku.ac.jp

Accepted 2009 September 22. Received 2009 September 17; in original form 2009 January 29

SUMMARY

Propagation of short period *S* waves through the crust is strongly controlled by scattering loss and intrinsic absorption. Scattering loss controls the shape of the seismic envelope and the spatial distribution of the energy while intrinsic absorption produces an exponential decay as a function of time which is independent of the coordinates. Since both parameters have a different effect, it is possible to compute them by means of the Multiple Lapse Time Window Analysis (MLTWA). In this paper, high resolution maps of Japan for both seismic *S*-wave attenuation parameters are obtained by using the MLTWA with data provided by the Hi-net seismic network. The maps show strong regional variation of the parameters. The variations depend mainly on the tectonic setting of each region and volcanism mechanisms. In the scattering loss maps, in the 1–2 Hz map, there is a very different behaviour between the northeast (stronger scattering loss) and the southwest (much weaker scattering loss). In the northeast of Japan, areas with strong scattering loss correspond mainly to the location of the volcanic arcs. In Southwest Japan, Chugoku region and the west side of Kii peninsula show strong scattering levels for the 4–8 Hz and higher frequency bands. In Hokkaido, strong scattering loss and intrinsic absorption can be observed for the lower frequency bands. In the Sendai plain, we find strong scattering loss for all the frequency bands. Under all these areas low velocity anomalies have been detected in previous works. In Tohoku area the east side shows lower intrinsic attenuation than the west side. This characteristic seems to extend to the southern part of Hokkaido and to central Japan. In Kanto area, the values of intrinsic absorption are lower than in the surrounding areas; but in the region around the Itoigawa-Shizuoka tectonic line and in its western side strong absorption areas are observed. The behaviour of each area for intrinsic absorption is similar to the behaviour observed in the Q_c^{-1} maps. The MLTWA is based on the hypothesis of multiple isotropic scattering in a medium with the homogeneous distribution of scattering mean free path and intrinsic absorption. Although these hypotheses are very simple, the results are very informative on the characteristics of each region, and show the usefulness of studying the properties of scattered seismic waves in the understanding of the properties of the crust.

Key words: Body waves; Seismic tomography; Seismic attenuation; Wave scattering and diffraction; Wave propagation; Crustal structure.

Q2

1 INTRODUCTION

After the 1995 Kobe earthquake, the Japanese government started to construct a dense and uniform network of strong motion, high-

sensitivity, and broad-band seismographs covering the whole country. Hi-net, which stands for high sensitivity seismograph network, presently consists of about 772 borehole-type seismic stations. To achieve high sensitivity and a high signal-to-noise ratio, seismographs are installed at the bottom of the borehole of about 100 m depth. Some reach depths of 3 km (Okada *et al.* 2004; Obara *et al.* 2005).

All the high sensitivity data including Hi-net and preexisting networks of Japan Meteorological Agency (JMA), University group

*Formerly at: Universitat Politècnica de Catalunya, Departament d'Enginyeria del terreny, Cartogràfica i Geofísica, Jordi Girona 1-3, Edifici D2, 08034 Barcelona, Spain.

(UNIV) and National Research Institute for Earth Science and Disaster Prevention (NIED) are collected by the NIED for archive of data and distribution to the public through their web page <http://www.hinet.bosai.go.jp/> (in Japanese) since 2002 June. These high quality data, combined with strong motion data provided by K-net and Kik-net are very useful not only for the study of seismicity and seismotectonics but also for the quantitative evaluation of earthquake strong motion. Precise mapping of seismic wave velocity has been done by applying tomography methods to onset readings of Hi-net data. See for example, Nakamura *et al.* (2008). For more precise description of wave propagation, it is necessary to establish the spatial distribution of scattering characteristics and attenuation especially for the quantitative prediction of earthquake motion in each region. There have been some studies on apparent seismic attenuation of S waves by Nakamura *et al.* (2006). Jin & Aki (2005) made a precise map of coda Q_c from the analysis of Hi-net data, which shows significant spatial variation and a strong frequency dependence.

In addition to seismic velocity, there are two key factors which characterize S -wave propagation: scattering coefficient g_0 which is a measure of medium heterogeneity and the scattering power per unit volume and intrinsic absorption Q_i^{-1} which changes the vibration energy into heat. We should note that the scattering coefficient is not only a measure of coda excitation but also a measure of the amplitude attenuation per travel distance; therefore, it is also convenient to define the scattering loss parameter Q_s^{-1} , which is given by

$$Q_s^{-1} = \frac{g_0 v}{\omega}, \quad (1)$$

where ω is the angular frequency and v is the S -wave velocity.

Detailed information on the attenuation structure provides insight into the nature of complexities in the Earth structure and composition. In this paper, we compute scattering loss Q_s^{-1} , intrinsic absorption Q_i^{-1} and the seismic albedo B_0 , which is the ratio of scattering loss to the total S -wave attenuation, by using the Multiple Lapse Time Window Analysis (MLTWA, Hoshiya 1991; Fehler *et al.* 1992; Sato & Fehler 1998) in Japan. This work may be considered a reappraisal or extension of the pioneer work done by Hoshiya (1993). In his paper, he showed strong regional dependence of attenuation parameters in Japan. However, density of the stations was very low (he used only 16 stations). In our case, we take benefit of the high quality Hi-net data in order to elaborate high resolution maps. Also coda attenuation Q_c^{-1} is computed for the same data set and results are compared with those from other attenuation parameters.

2 DATA AND METHOD

For this study, we have collected Hi-net data from more than 135 000 events with magnitudes higher than 1.5 and maximum 3.5 within the period 2002 June–2007 December. Hi-net stations uniformly cover the Japanese Islands with a spacing of 20–30 km, allowing us to plot high resolution maps (see Fig. 1 for the location of hypocentres and stations and Fig. 2 for the main topographic features of the islands). From each station we obtained data for the three components and the records provide signals sampled at a 100 Hz rate. For every station, we collected events within a radius of 100 km and a maximum depth of 40 km. At least 20 events have been collected at every station to perform each calculation. If a smaller amount of data is available calculations are not performed. Then, our results show

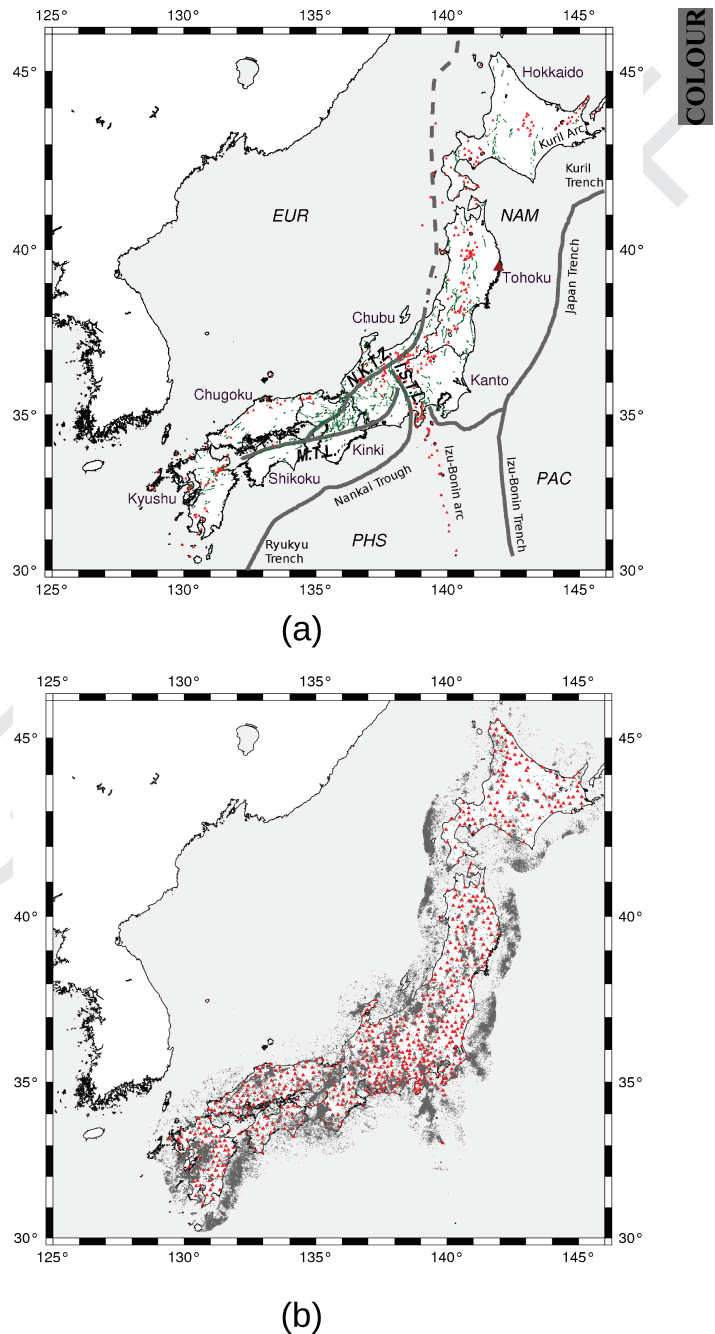


Figure 1. In (a) location of the main Quaternary volcanoes (red triangles), tectonic lines (black lines), tectonic plate boundaries and major tectonic lines (grey lines) are indicated in the map. Names of the main areas in Japan are also written. The following notation is used: PHS: Philippine Sea Plate, PAC: Pacific Plate, NAM: North American Plate, EUR: Eurasian Plate, NKTZ: Niigata to Kobe Tectonic Zone, ISTL: Itoigawa-Shizuoka Tectonic Line, MTL: Median Tectonic line. Information of active faults are from Nakata, T. and Imaizumi, T. (2002). In (b), the locations of the Hi-net stations used in this study are indicated by small triangles and the events with magnitudes higher than 1.5 and lower than 3.5 are depicted as grey dots.

lateral variations of the average properties of the crust around each station.

In this paper, we consider the square sum of the three component amplitudes of the incoming S waves and the following coda as a measure of the energy arriving to the station. Then, a single



Figure 2. Topographic map of Japan. The names and location of some mountains, ranges and plains cited in the main text are indicated. The extension of the Beppu-Shimabara Grabben is indicated by dashed lines. The MTL and ISTL show up as topographic features.

energy envelope, representing the total energy arriving to each station is considered for each event. From this envelope, attenuation parameters are evaluated.

2.1 Multiple Lapse Time Window Analysis

The MLTWA is a method to analyse the seismic time traces taking into account that their characteristics strongly depends on Q_s^{-1} and Q_i^{-1} (e.g. Hoshiya 1991; Fehler *et al.* 1992; Hoshiya 1993; Sato & Fehler 1998). In order to determine the values of Q_s^{-1} and Q_i^{-1} , it is very convenient to consider the logarithm of the integral of the energy on a certain number of time windows. Usually, three windows are considered, although a larger number could be used at the expense of a longer computation time. The length of the windows is in most cases taken as approximately 15 s. Q_s^{-1} and Q_i^{-1} determine how the energy is distributed in each window and its dependence with the hypocentral distance. Each parameter has a different influence. When scattering is weak, most of the energy is concentrated in the first window. However, as stronger scattering

values are considered, more energy is accumulated in the second and third windows at the cost of the energy in the first window. If we consider different distances, the ratio at which the energy should increase for the second and third window strongly depends on the value of Q_s^{-1} . Intrinsic absorption Q_i^{-1} produces a linear decay on time of the logarithm of the energy of the seismic wavefield which is independent on the coordinates. Then, its effect is mainly to produce a linear decay on the logarithm of the energy of every window as a function of hypocentral distance. Then, the study of the logarithm of the energy for each window versus hypocentral distance provides an ideal framework that allows separating the influence of each attenuation parameter.

In order to determine the parameters, it is necessary to compare the observed results with the ones provided from a certain theoretical model. If we assume an infinite extent media of constant characteristics and isotropic scattering, it is possible to derive an approximate analytic expression for the energy density of the time traces $P(r, t)$ for a unit energy source radiation, as a function of the hypocentral distance r , the scattering loss Q_s^{-1} and intrinsic

absorption Q_i^{-1} the S -wave velocity v and the frequency ω :

$$P(r, t) \simeq \frac{1}{4\pi r^2} \delta(r - vt) \exp[-\omega t (Q_s^{-1} + Q_i^{-1})] \\ + \frac{(1 - r^2/v^2 t^2)^{1/8}}{(4\pi Q_s v^2 t/3\omega)^{3/2}} \exp[-\omega t (Q_s^{-1} + Q_i^{-1})] G \\ \times \left[\omega t Q_s^{-1} \left(1 - \frac{r^2}{v^2 t^2}\right)^{3/4} \right] \Theta(vt - r) \\ G(x) = 8(3x)^{-3/2} \sum_{N=1}^{\infty} \frac{\Gamma(\frac{3}{4}N + \frac{3}{2}) x^N}{\Gamma(\frac{3}{4}N) N!}. \quad (2)$$

This approximate expression was derived by Paasschens (1997) and has an accuracy higher than 3% for the onset and the following coda. The exact solution is a double integral expression derived previously by Zeng *et al.* (1991). Then, for each hypocentral distance, we can compute the three integrals for this expression and compare this synthetic result with the observed ones for different values of Q_s^{-1} and Q_i^{-1} and thus carry out a fitting process with a least-squares algorithm. Eq. (2) has been previously used by Abubakirov (2005) to perform this kind of analysis. The fitting process is usually performed by using a least-squares algorithm.

We explain now in some detail our implementation of the MLTWA. We consider a single station for each calculation. For each event located at a certain hypocentral distance r_i , the addition of the mean squares of amplitudes of each component, within a lapse time of 45 s, measured from the onset of S waves, is computed. It should be noted that we only consider time traces with signal-to-noise ratio higher than 3 for the three windows. Then, we use the same amount of data for each window. This is convenient since lateral variations in Japan are sometimes strong and it is important to make sure that the same amount of information is contained in each window. With this criteria more than 190 000 useful time traces were obtained.

To filter the envelopes, we use bandpass Butterworth filters of order 3, back and forth, to avoid phase delays. We consider the following frequency bands: 1–2, 2–4, 4–8, 8–16 and 16–32 Hz. We remark here that after the filtering process we keep a 100 Hz sampled signal. Previous to filtering, we assigned zeroes for times smaller than the arrival of the S wave in order to avoid further contributions from P waves. This way, for the first time window, the integration process may start -1 s before the arrival of the S wave in order to take into account correctly the energy contained in the first window (Hoshiba 1993). We consider three 15 s time windows in total. We carry out the integral of the energy contained in each window and we call them $U_{i,j}$, where $j = 1, 2, 3$ indicates the window. We normalize each integral by dividing the signal with the integration window of ± 5 s around $t_{\text{ref}} = 65$ s. We call this normalization factor $U_{i,4}$. This way we correct for the source power and local amplification at each station (Aki 1980). We correct for geometrical spreading with a $4\pi r_i^2$ factor. For each window we consider then the logarithm of the total energy contained in each window. In order to fit the attenuation parameters we define the following merit function

$$\chi^2(Q_s^{-1}, Q_i^{-1}) = \sum_i \sum_j \left[\log \left(4\pi r_i^2 \frac{U_{i,j}}{U_{i,4}} \right) - \log \left(4\pi r_i^2 \frac{P_{i,j}(Q_s^{-1}, Q_i^{-1})}{P_{i,4}(Q_s^{-1}, Q_i^{-1})} \right) \right]^2 \\ \chi^2(Q_s^{-1}, Q_i^{-1}) = \sum_i \sum_j \left[\log \left(\frac{U_{i,j} P_{i,4}(Q_s^{-1}, Q_i^{-1})}{P_{i,j}(Q_s^{-1}, Q_i^{-1}) U_{i,4}} \right) \right]^2, \quad (3)$$

where $P_{i,j}(Q_s^{-1}, Q_i^{-1})$ is the integral for each window computed with the synthetic envelope given by (2) and $P_{i,4}(Q_s^{-1}, Q_i^{-1})$ is the corresponding normalization factor. We remark here that a 100 Hz sampled synthetic envelope is considered in order to carry out the integration in the same way as with the observed envelopes for the consistency of the fitting process. In order to evaluate (2) a different single average S -wave velocity is used for every station. To estimate the velocity, the average S -wave velocity around the region of every station we consider the ratio of the hypocentral distance and the S -wave arrival time for each event and then we average all the ratios. Although this method of calculating average S -wave velocities only considers the path of the direct waves, it allows taking into account easily regional variations of the average velocity. Since gradients of velocity are sometimes noticeable, we considered that it is better to work with this estimate rather than working with a single average velocity through all Japan as in Hoshiba (1993).

We need now to implement a fast and reliable algorithm to minimize χ^2 in order to compute attenuation parameters for a very large number of data sets. Usually, a grid search method is used to determine the attenuation parameters. However, the grid search method is not a fast method and the accuracy is limited by the size of the grid. In the literature and in common software packages there are robust, efficient and accurate techniques to carry out non-linear least-squares fitting, as the well-known Levenberg–Marquard algorithm. The Levenberg–Marquard algorithm is a wise combination of the steepest descent and the Gauss–Newton algorithms (Press *et al.* 2007) and it is much faster and exact than a grid search. Moreover, it provides a linear estimate of the errors of the parameters from the values of the variance–covariant matrix. In Fig. 3, we show an example of data and the best-fitting curves for the Hi-net station N.YMDH located in the northeast Japan for all the frequency bands considered in this paper. The location of the station is indicated in Fig. 1(a) by a triangle in Tohoku area.

Q4

2.2 Coda attenuation Q_c^{-1}

In this paper, we would like to analyse the overall decay of coda power envelope at frequency f , measured by Q_c^{-1} by using the single scattering model

$$P(r, t) \propto \frac{1}{t^2} e^{-Q_c^{-1} 2\pi f t} \quad (4)$$

and compare it with the results for Q_i^{-1} and Q_s^{-1} . With this in mind, we would like to discuss here the importance of lapse time in the measurement of Q_c^{-1} . It has been reported previously the dependence of Q_c^{-1} with lapse time (see Yoshimoto & Jin 2008 and references there in). With increasing lapse time, Q_c^{-1} approaches a constant value at a lapse time of about 24 s, at least for shallow events (depth < 23 km) in Nagano, Japan (Kosuga 1992). However, this lapse time depends on the frequency band and the location and depth of events.

There are previous measurements of Q_c^{-1} in Japan considering different lapse times. In order to compare Q_c^{-1} with Q_i^{-1} and Q_s^{-1} , Hoshiba (1993) used the measurements of Q_c^{-1} from Hoshiba & Goto (1988). In this paper, they considered only vertical components, focal depths less than 60 km and epicentral distances less than 120 km. A time window of $2r/v$ to $2r/v + 40$ s from the origin time was adopted. Results are listed in Hoshiba (1993) for all the parameters. Q_c^{-1} was also measured later on using Hi-net data by Jin & Aki (2005). They used very different conditions. They used events located within 30 km from the stations. The lapse time was

COLOUR

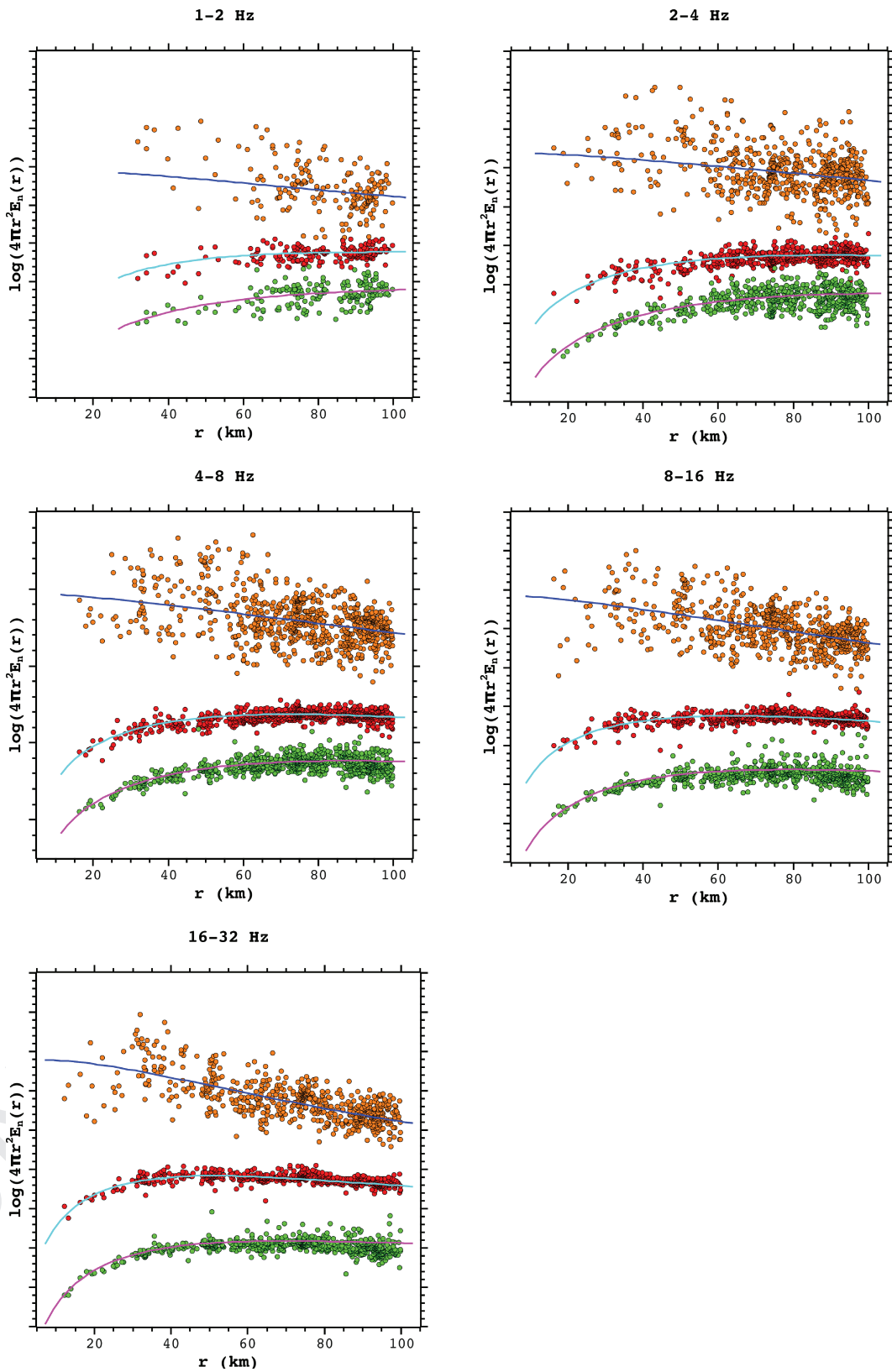


Figure 3. Example of MLTWA. Data and the best-fitting curves for the Hi-net station N.YMDH located in the northeast Japan for all the frequency bands. Orange, red and green points correspond to the first, second and third window, respectively. The continuous lines corresponds to the fitting carried out by using a synthetic model. The location of the station N.YMDH is indicated in Fig. 1(a) by means of red triangle.

restricted within 30 s from the origin time. They computed then Q_c^{-1} averaging over the three components.

In our paper, we computed Q_c^{-1} using closer conditions to the work of Hoshiha (1993). In our case, we consider hypocentral distances within 100 km. The portion of the time trace used to compute Q_i^{-1} and Q_s^{-1} ranges from the *S*-wave onset, r/v and has a total duration of 45 s. Since coda decay depends on the lapse time, and we wish to compare the coda decay Q_c^{-1} with the corresponding values of Q_i^{-1} and Q_s^{-1} , we have to consider a similar portion of the time trace to compute Q_c^{-1} . Then, we compute Q_c^{-1} from $2r/v$ up to $r/v + 45$ s from the origin time. This procedure ensures that at least 20 s are considered to measure Q_c^{-1} . It also ensures the consistency between the measurement of coda decay Q_c^{-1} and the measurements of Q_i^{-1} and Q_s^{-1} as in Hoshiha (1993).

To compute Q_c^{-1} from every waveform, we compute the smoothed trace of the square sum of the three components of the seismograms (MS seismogram envelope) and followed the same process as in the last subsection to obtain the envelopes. After filtering, to compute Q_c^{-1} , the envelopes are slightly smoothed via convolution with a rectangle function. The time length of the window defined with the rectangle function is different for each frequency band. We consider smoothing as an important step that has to be done carefully. If we choose a wide smoothing window, the signal will be distorted and decay ratio may be altered, since we are dealing with an exponentially decaying signal. If we choose a too much small smoothing window, the small values (near zero) will take too much importance when the logarithm is taken to compute Q_c^{-1} . In the literature, different authors use different smoothing windows in their studies. We choose the following smoothing windows: 2 s for 1–2 Hz; 1 s for 2–4 Hz; 0.5 s for 4–8 Hz; 0.25 s for 8–16 Hz; 0.12 s for 16–32 Hz. Our criterion is to take a time that corresponds to twice the period of the first corner frequency of each band (or four times the period of the second corner frequency). After taking the logarithm of the smoothed envelope, a rippled signal is obtained that decays linearly in time. We notice in here that we keep a 100 Hz sampled signal after filtering, smoothing and taking the logarithm. This way we keep a time trace that still corresponds to the original one. Afterwards, the corresponding linear regression is taken in order to estimate Q_c^{-1} . The process of performing a linear fitting is a smoothing process all by itself. Then, the process of obtaining Q_c^{-1} really involves two smoothing processes.

2.3 Mapping

The results of every attenuation measurement is assigned to the coordinates of each station. This is an important decision since we wish to show the dependency of the results with the location of the station used to perform each measurement. The result in each station should represent an average of the attenuation parameters around the station. Taking into account that the maximum hypocentral distance under consideration is 100 km and the maximum depth is 40 km, this is quite a large volume of about 100 km depth (in the single scattering approximation). From this fact it seems that the variation of the parameters should be smooth. However, in Japan, due to arc volcanism and the subduction of tectonic plates, lateral variations are strong, as shown by many previous studies based on different techniques, as seismic velocity tomography. This means that the characteristics of the environment of each station may rapidly change as a function of the coordinates and it makes necessary to assign each measurement to the coordinate of the corresponding station. Then, in the maps, for certain regions noticeable gradients will be observed.

Mapping the results has been performed by means of GMT routines. Specification of values of parameters used in the GMT routines is provided in Appendix A to allow readers to reproduce similar maps in the future. Also some technical details are briefly commented.

3 BASIC CHARACTERISTICS OF THE ATTENUATION MAPS. COMPARISON WITH PREVIOUS WORKS

The attenuation maps and the corresponding frequency dependence are depicted in Figs 4–7, for Q_i^{-1} , Q_s^{-1} , B_0 and Q_c^{-1} . The frequency dependence of the attenuation parameters for each region is quantified by fitting to the form $Q^{-1} = Q_0^{-1} \cdot f^{-\gamma}$ for each station. The exponent γ is plotted then for Q_i^{-1} , Q_s^{-1} and Q_c^{-1} as a measure of frequency dependence and it has been computed only when we had information for all the frequency bands. An estimation of the errors by using the variance–covariance matrix of each fitting is reported for Q_i^{-1} and Q_s^{-1} for each frequency band in Figs B1 and B2 in the Appendix B. In each map, the location of Quaternary volcanoes and the main faults are also drawn. It is possible to observe a strong dependence of the values of the parameters with the coordinates for all the frequency bands in some regions.

In Section 4, we describe the results in detail. We shall provide now a brief description of the most striking, gross features that can be observed in the maps. In the scattering loss maps, we can observe that in the 1–2 Hz map, there is a very different behaviour between the northeast (stronger scattering loss) and the southwest (much weaker scattering loss). In the northeast of Japan, areas with strong scattering loss correspond mainly to the location of the volcanic arcs. In southwest Japan, Chugoku region and the west side of Kii peninsula show strong scattering levels for the 4–8 Hz and higher frequency bands. In Hokkaido, strong scattering loss and intrinsic absorption can be observed for the lower frequency bands. In the Sendai plain, we find strong scattering loss for all the frequency bands. Under all these areas strong low velocity anomalies exist as we point out in detail in the next section. In Tohoku area the east side shows lower intrinsic attenuation than the west side. This characteristic seems to extend to the southern part of Hokkaido. It also extends to central Japan, in Chubu area and Kanto area. In Kanto area, the values of intrinsic absorption are lower than in the surrounding areas; but in the region around the Itoigawa-Shizuoka tectonic line and in its western side strong absorption areas are observed. The behaviour of each area for intrinsic absorption is similar to the behaviour observed in the Q_c^{-1} maps.

The mapping of the estimate of the errors does not show a random distribution. The mapping of the estimate of the errors shows region dependent distributions that seem to provide information about both the scattering and absorption phenomena. It is tempting to interpret the errors associated with the measurement of the attenuation parameters in terms of the degree of heterogeneity of the media. However, there are many kinds of heterogeneities in the crust of Japan, so it is difficult to establish the meaning of ‘degree of heterogeneity’ for each region.

In order to show consistency with previous results obtained in similar conditions, we would like to show a comparison between Hoshiha (1993) and our results obtained with Hi-net data for Q_i^{-1} , Q_s^{-1} and Q_c^{-1} . It is the only source that allows us comparing, simultaneously, all the parameters calculated by means of a very similar analysis in different regions of Japan. The comparison is shown in Appendix B for the three frequency bands and the 16 JMA’s stations

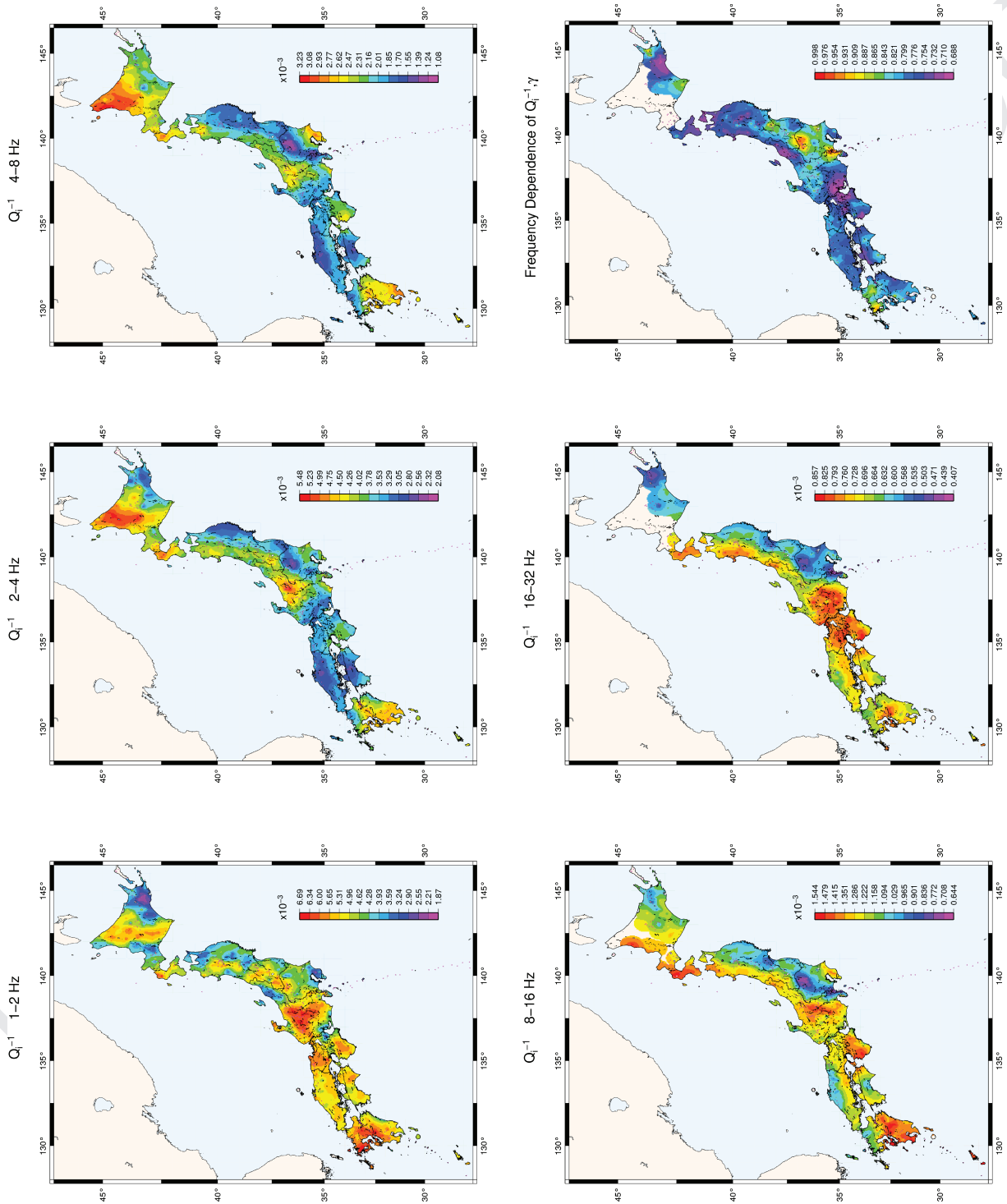


Figure 4. Graphical representation of intrinsic absorption Q_i^{-1} values for all Japan. Quaternary volcanoes are indicated by means of purple triangles and main faults are indicated by means of black lines in this map and in all the maps that follows. The scale indicates the maximum and minimum values obtained for each frequency band.

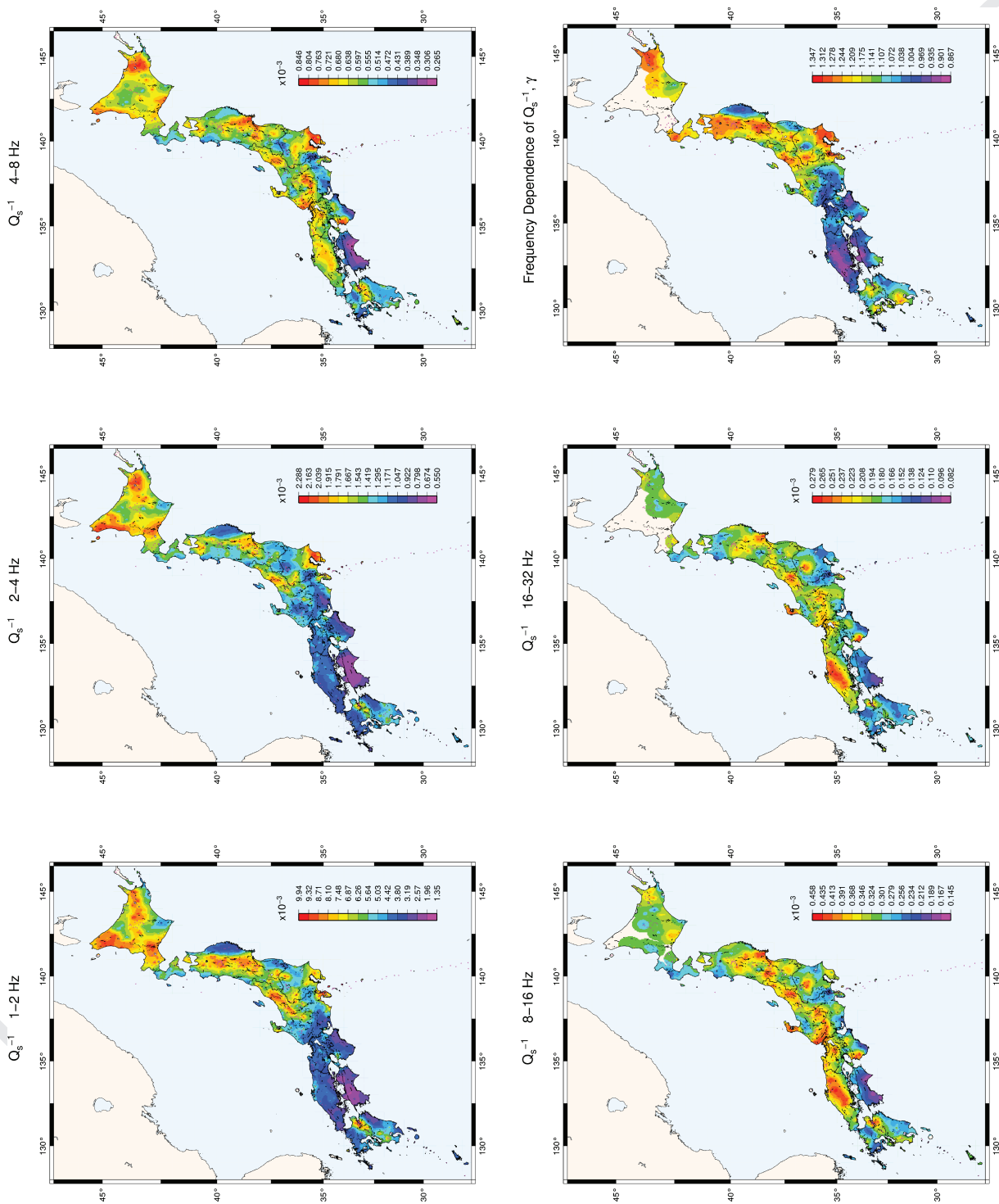


Figure 5. Graphical representation of scattering loss Q_s^{-1} values for all Japan.

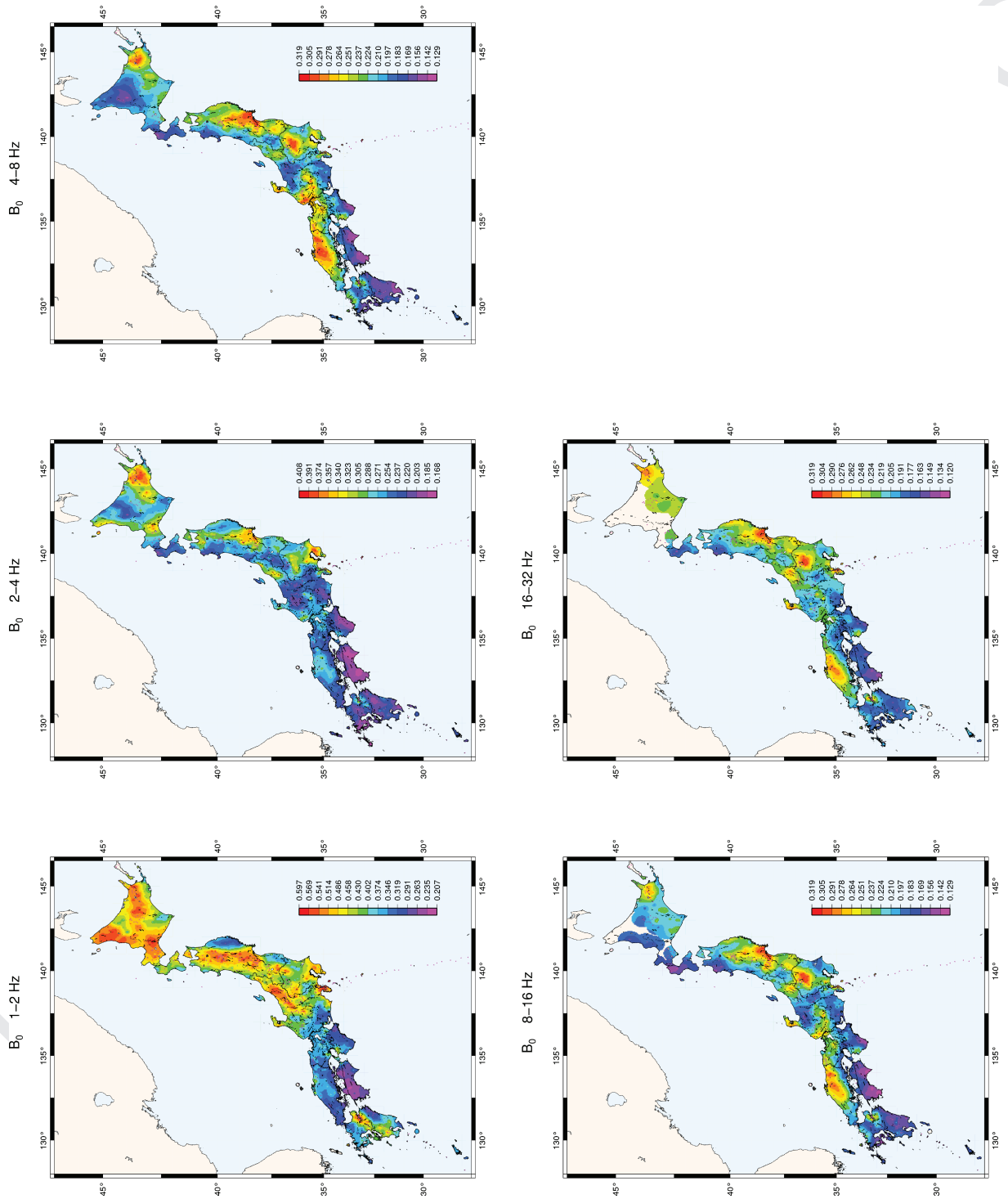


Figure 6. Graphical representation of seismic albedo B_0 values for all Japan.

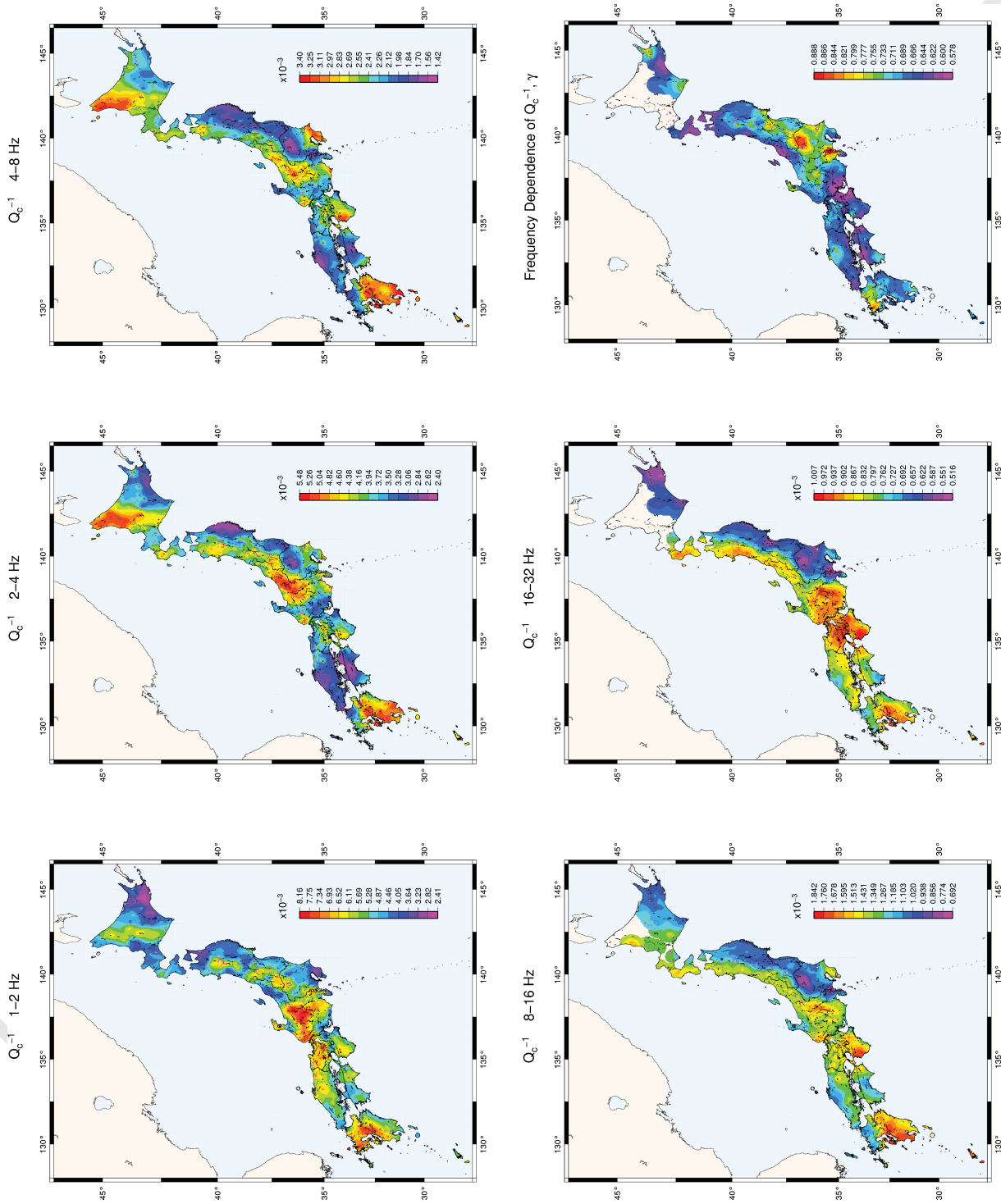


Figure 7. Graphical representation of Q_c^{-1} values for all Japan.

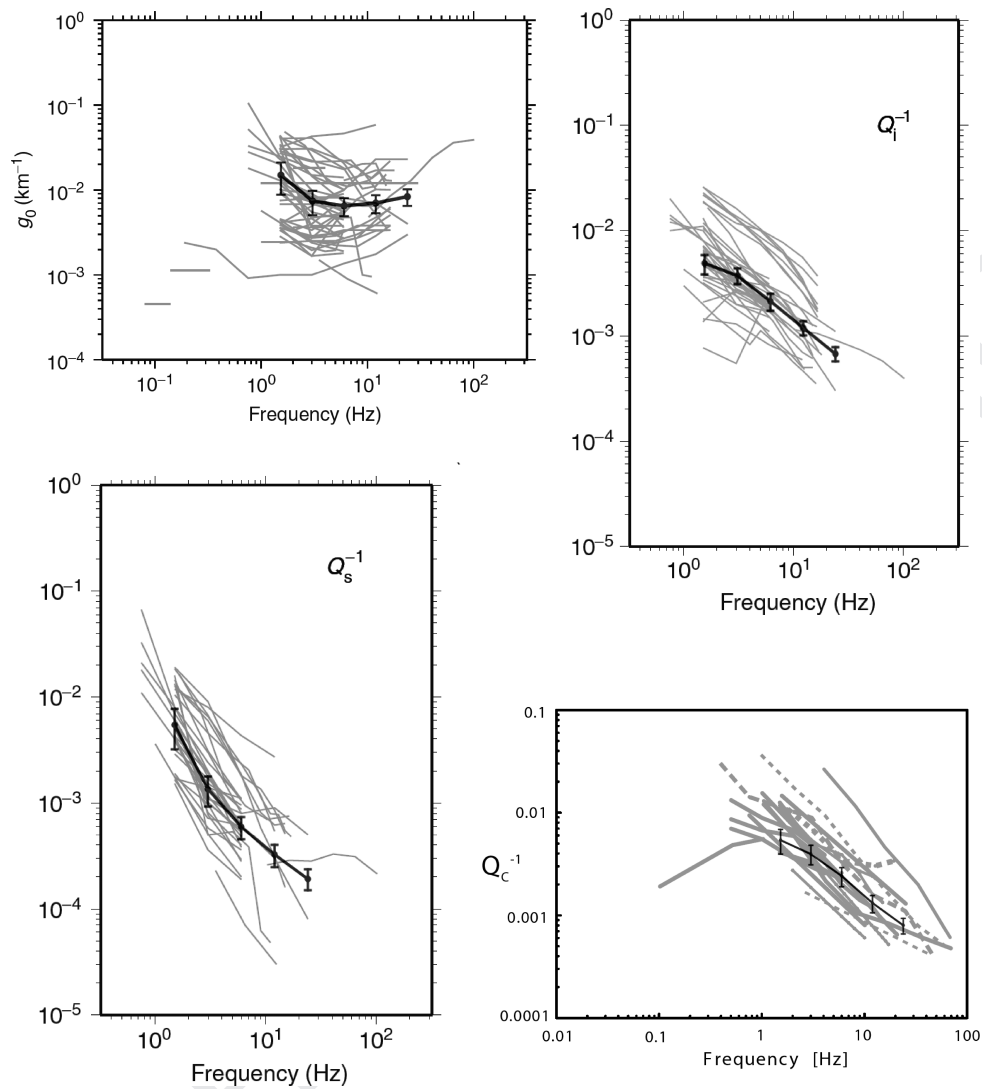


Figure 8. Graphical representation of the mean values and standard deviation (error bars) of g_0 , Q_s^{-1} , Q_i^{-1} , Q_c^{-1} for all Japan and other regions of the world (grey lines). The grey lines were obtained from Yoshimoto & Jin (2008).

used in Hoshiya's paper. The correlation with our results seems quite satisfactory taking into account the differences of instruments and data set.

In Jin & Aki (2005) different conditions were used to compute Q_c^{-1} as already discussed in the previous section. To compare exact values from both results is quite difficult; however, differences in the results are clear in some regions. Differences also depend on the frequency band. For instance, in the 16–32 Hz band we obtain different behaviours in each region, but in their results all Japan Islands show up as an homogenous area. These differences point out the importance of lapse time in the computation of Q_c^{-1} . However, some important common points can be found. In the 1–2 Hz and in 2–4 Hz frequency band Q_c^{-1} have high values on the Niigata Kobe Tectonic Zone (NKTZ). In the 2–4 Hz and 4–8 Hz the lowest values of Q_c^{-1} are in Chugoku and Shikoku regions and also in the east side of Tohoku area. In the 4–8 Hz map, in Central Japan, high values are observed in northern Fossa magna; in Kanto area, the region with lowest values of Q_c^{-1} is also common. In the 4–8 and 8–16 Hz band it is possible to observe that Kyushu shows higher values than Chugoku and Shikoku regions and that Q_c^{-1} is higher in the west side of Tohoku than in the east side.

In Fig. 8, we compare our results with other results obtained around the world plotted in [Sato & Fehler \(1993\)](#) and [Yoshimoto & Jin \(2008\)](#). We plot the average value of each parameter for each frequency band and the corresponding standard deviation indicated by means of error bars. These graphics show the overall frequency dependence of g_0 , Q_s^{-1} , Q_i^{-1} and Q_c^{-1} . g_0 shows a minimum value for 4–8 Hz band. It can be seen that Q_c^{-1} and Q_i^{-1} show a similar pattern, at that scattering has a higher importance than intrinsic absorption for the lowest frequency band.

In the following, we shall describe the structure of our maps depicted in Figs 4–7 by regions. For every region, the main geotectonic characteristics are introduced. Then, the results in our maps are explained in correspondence with the available information of each area.

4 CHARACTERISTICS OF THE ATTENUATION MAPS

Here, for each region of Japan, we describe the resultant characteristics of attenuation in relation with the seismotectonical setting and

Q5

other previous studies, including seismic tomography and strain rates measured by the GPS Earth Observation Network of Japan (GEONET), which includes more than 1200 GPS stations with an average distance of 20 km (Sagiya *et al.* 2000). Surface deformation is closely related to tectonic activity and internal mechanical processes of the crust, which may affect the propagation of the seismic waves.

The following tectonic plates exist in and around Japan: the North American Plate (NAM), the Eurasian Plate (EUR), the Philippine Sea Plate (PHS) and the Pacific Plate (PAC) (see Fig. 1). The regional stress field caused by the motions and interactions of these plates produces intense seismic and volcanic activities and active crustal movement beneath Japan. Two of the plates subduct beneath the Japan Islands. One is the PAC moving towards the west and subducting into the mantle with a dip angle of about 30° and at a rate of about 80 mm yr⁻¹ from the Japan Trench relative to the NAM. The other is the PHS moving to the northwest. This complex setting originates strong lateral variations of the properties of the crust and a complex geological setting that is different for every region of Japan. Fig. 2 contains the names of the main topographic features used in description and discussion of the results.

4.1 Hokkaido

4.1.1 Geological and tectonic setting of Hokkaido

The northern island of Japan, Hokkaido, is located at the conjunction of two active island arc–trench systems; the Northeast Honshu Arc–Japan Trench and the Kuril Arc–Trench. Hokkaido is divided into three major regions with regard to its geology, Western, Central and Eastern Hokkaido, (Arita *et al.* 1998; Itoh *et al.* 2005; Ueda 2005). *Central Hokkaido* has been occupied by two subduction–accretion systems between the palaeo-Eurasian and palaeo-North American plates; the first one is a N–S-trending, westward-subducting system of Late Jurassic to Palaeogene age, and the second one in the east is an eastward-subducting system of Cretaceous age (Kato *et al.* 1990). Central Hokkaido has undergone two stages of collisions since the Early Tertiary. The process of collision is still continuing and the Hidaka Mountains and their surroundings are therefore collectively termed as the ‘Hidaka Collision Zone’ (HCZ). In Western Hokkaido there is a depression zone located to the west of the central collision zone. The Oshima Peninsula can be considered from a geological point of view as a northern extension of the northeast region of the Honshu island. Eastern Hokkaido is in the Kuril Arc, and it is divided into a forearc and an backarc by the east–west oriented volcanic front. In the forearc there are lowlands as the Konsen plateau and the Kushiro plain composed of Quaternary sedimentary rocks.

Hokkaido is under compression due to the subduction of the PAC (Sagiya *et al.* 2000; Toya & Kasahara 2005). Strong strain rates have been measured along the volcanic front in eastern Hokkaido and also in the southwest of the HCZ. Strong shear and rotational strain rates have been detected in the volcanic front of eastern Hokkaido and in the Hidaka Range.

4.1.2 Characteristics of the attenuation maps

Intrinsic absorption. For the band of 1–2 Hz, the region of central Hokkaido shows up as a region of quite strong intrinsic absorption ($Q_i^{-1} \approx (5.0 - 6.0) \times 10^{-3}$). The main active faults follow this orientation. The southwest and southeast sides of the band seem lim-

ited by active faults. The lowest values of intrinsic absorption in Japan are located in the low-lands of southeastern Hokkaido Island for this frequency band $Q_i^{-1} \approx 1.9 \times 10^{-3}$. For the frequency bands of 2–4 Hz intrinsic absorption reaches the highest values $Q_i^{-1} \approx 5.5 \times 10^{-3}$ as well as for the frequency band of 4–8 Hz $Q_i^{-1} \approx 3.2 \times 10^{-3}$ in the north side of Central Hokkaido. The behaviour of the attenuation in Oshima peninsula (southwest edge of Hokkaido Island) is quite similar to the north of Tohoku for the lowest frequency bands; a portion of the volcanic front shows up as a high absorption area for all the frequency bands. Low attenuation values are observed in the southeast, in the low lands.

Scattering loss. The volcanic front clearly appears in our maps in the band of 1–2 Hz. Also, a north–south belt shows up as a strong scattering structure in the map. Main values concentrate in a wide region of the north and in a more reduced area in the south, in coincidence with a region with active faults reaching a maximum value of ($Q_s^{-1} \approx 10 \times 10^{-3}$). As the frequency increases, the high scattering zone corresponding to the volcanic front concentrates in the eastern volcanic area up to the band for 4–8 Hz, and disappears for higher frequencies. This region shows very high strain ratios contractional, shear and rotational (Sagiya *et al.* 2000; Toya & Kasahara 2005). It also shows the highest albedo values in Hokkaido for most frequency bands. For the 2–4 Hz frequency band it reaches the maximum value in Japan $B_0 \approx 0.4$. In the band of 1–2 Hz albedo has noticeable values in both the volcanic arc and the north–south structure. The north–south structure reduces its size to the west side and vanishes as frequency increases. It is remarkable that the region of the Hidaka Mountains show low scattering values for all the frequency bands.

Coda attenuation Q_c^{-1} . For the band from 1 to 2 Hz, the region of central Hokkaido shows up as a region of moderate coda attenuation. Very weak attenuation can be observed in the low-lands of southeastern Hokkaido Island $Q_c^{-1} \approx 2.4 \times 10^{-3}$.

For the frequency bands of 2–4 and 4–8 Hz the north side of Central Hokkaido reaches the highest attenuation values $Q_c^{-1} \approx 5.5 \times 10^{-3}$ and $Q_c^{-1} \approx 3.4 \times 10^{-3}$, respectively. The behaviour of the attenuation in Oshima peninsula is quite similar to the north of Tohoku. Lowest attenuation values are observed in the southeast.

4.2 Tohoku

4.2.1 Characteristics of the region

The Tohoku region belongs to the Northeastern Japan Arc which lies to the west of the Japan Trench where the PAC descends beneath the NAM (Hashimoto & Matura 2006). The tectonic structure of northeast Japan is characterized by the thrust folds and folds with their strikes parallel to north–south direction (Sato 1994). This suggests long-term duration of east–west compression, as reported by Sagiya *et al.* (2000). The Northeastern Japan Arc is divided into a forearc (east side) and backarc (west side). Major features of the forearc are the Kitakami Mountains and the Abukuma Mountains, and those of the backarc are the Ou Range, the Dewa Mountains, and the Iide Mountains. The Ou Range runs north to south over about 500 km in the centre of the island arc—the longest range of Japan—but its width is narrow (about 35 km). The range contains a single north–south ridge with Quaternary volcanoes comprising a volcanic front. Below the backarc, upwelling of aqueous fluid from the mantle to the crust occurs (Hasegawa *et al.* 2005). This upwelling is related with the partial melting of material below the Moho. The flow of this material reaches the Moho just below the volcanic front.

Several studies have been performed in order to study the presence of arc magma and fluids under the central part of northeastern Japan (Nakajima *et al.* 2001a,b). These studies determined that partial melting of materials exist in the uppermost mantle along the volcanic front and they spread up to the midcrust of the volcanic areas. In the upper crust of the volcanic areas, water rather than melt exist there. Strong strain rate have been measured in the southern part of the volcanic front of Tohoku (Toya & Kasahara 2005).

4.2.2 Characteristics of the attenuation maps

Intrinsic absorption. In the intrinsic absorption maps, two main facts can be observed, the volcanic front and a clear difference between the backarc (west side) and forearc (east side) behaviour. In the 1–2 Hz band the volcanic front shows up. However, it does not appear as a uniform north–south axis and shows a complex structure in contrast with the behaviour of the scattering loss and seismic albedo maps. Absorption is clearly weaker in the forearc than in the backarc for all frequency bands. In order to show the frequency dependence of this different behaviour, in Fig. 9, we plot the values of intrinsic absorption for all stations located in a region between 39° and 40° latitude against of the longitude. For 1–2 Hz maximum values correspond to the volcanic arc for a longitude of about 140.5°. For a higher longitude of about 140.75°, a sudden decrease is observed in all frequency bands, which indicates the border between the forearc and the backarc behaviour.

Scattering loss. Higher values of Q_s^{-1} are obtained along the volcanic arc for (1–2 Hz) in correspondence with the nature of this area. There is a clear and wide north–south high scattering band following the orientation of the main faults in Tohoku area. Also the seismic albedo shows an analogous behaviour. A low scattering/albedo zone corresponding to Kitakami Mountains can be seen for this frequency band and for the 2–4 Hz band. No active faults

lie in this area. In the 2–4 Hz band, Q_s^{-1} has the highest values in the Sendai plains and the portion of the volcanic front next to it. This region corresponds to maximum strain rates in Tohoku (Toya & Kasahara 2005). As frequency increases, this strong attenuation region, which also shows high albedo values, extends to the northwest. In Tohoku, Q_s^{-1} has its smallest values in the 1–2 and 2–4 Hz band in coincidence with the Kitakami range.

Coda Q_c^{-1} . In the 1–2 Hz band the volcanic front on the Ou range becomes clearly visible in the map. For all frequencies, lowest values of attenuation are found mainly in all the regions where the Pacific slab has less than 100 km depth (Nakamura *et al.* 2008). This behaviour can be also observed in the intrinsic absorption maps. This line does not only define a good portion of the forearc of northeast Japan, but also defines a low attenuation zone through Kanto area and Hokkaido island. The Akita basin and Niigata basin (Chubu) show low attenuation in the 1–2 Hz frequency band. In Jin & Aki (2002) it can also be observed that Q_c^{-1} is higher in the back arc for 2–4, 4–8 and 8–16 Hz, although the difference is not so clear as in our case. We also find a different frequency dependence for the back arc and forearc that is not detected in Jin & Aki (2005).

4.3 Central Japan (Chubu, Kanto)

4.3.1 Geological and tectonic setting of central Japan

Three arcs, the ‘Northeastern Japan Arc’, the ‘Southwestern Japan Arc’ and the ‘Izu-Bonin Arc’, meet in the central part of Honshu. In Kanto region, the PAC subducts from east and the PHS subducts from southeast.

The Itoigawa-Shizuoka Tectonic Line (ISTL) is the border between the EUR and the NAM and it runs north to south in central Honshu. Then, it divides Honshu into the Southwestern Arc and the Northeastern Japan Arc. The ISTL is an active fault system with the largest slip rates (4–9 mm yr⁻¹) in Japan (Sato *et al.* 2004). A zone in the northeast of the Itoigawa-Shizuoka Tectonic Line (ISTL) is called ‘Fossa Magna’. The volcanic front which extends from Northeastern Japan turns southward at the Fossa Magna and continues toward the Izu-Bonin Arc from north to south crossing over Honshu Island. On the western side of the ISTL there are three important ranges. From north to south, we have the Hida Range, the Kiso Range and the Akaishi Range. This region is intensely uplifted and there are many active faults. Central Japan accumulates the largest number of faults in Japan. The Median Tectonic Line (MTL), which is the longest tectonic line in Japan, (about 1000 km) runs from eastern Kyushu to the Kinki region, and curves to the northeast in the Chubu region where it coincides with ISTL.

We pay special attention to the Hida range, since several important seismological studies have been conducted in this area (Aoyama *et al.* 2002). The northern part consists of several peaks rising 3000 m above the sea level. The uplift of this area began in the late Tertiary and continued through the Quaternary (Fukao & Yamaoka 1983). Geological studies reveals many faults in these mountains (Yamada *et al.* 1989), indicating that the deformation of the Hida Mountains is very large and progresses rapidly. The seismological surveys of crustal structure beneath the Hida Mountains reveal the existence of a low Q and a low velocity anomaly beneath the main range at a depth of ~10 km below sea level (Katsumata *et al.* 1995; Matsubara *et al.* 2000). These results may suggest the existence of a partially molten region under the Hida Mountains as suggested by Mizoue *et al.* (1983), Katsumata *et al.* (1995) and Yamazaki (1996).

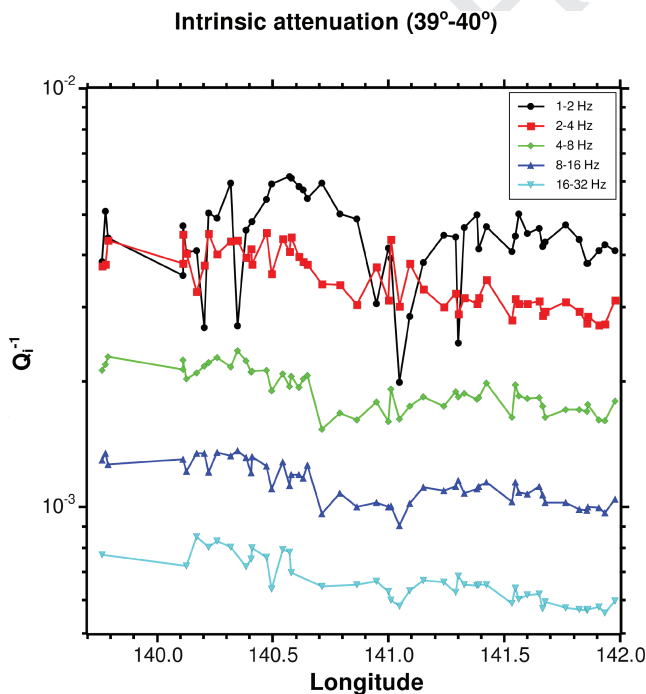


Figure 9. Values of intrinsic absorption Q_i^{-1} for all the frequency bands and for all stations located in a region between 39° and 40° latitude as a function of the longitude. This graphic illustrates the differences between the east and west side of Tohoku area.

The Kanto Plain, which is the largest plain in Japan, expands to the east of the Kanto Mountains, where there is a broad depression area. The Izu Peninsula, located to the south of the Kanto Mountains, is a block of the Izu-Bonin Arc accreting to and colliding with the Honshu Arc. Mt Fuji, the largest basaltic stratovolcano in Japan is located to the north of Izu peninsula.

There is a high-strain rate band crossing central Japan from Niigata to Kobe. Tada, Sagiya and Miyazaki (Tada *et al.* 1997; Sagiya *et al.* 2000) proposed to call this zone as the Niigata-Kobe Tectonic Zone (NKTZ) (see Fig. 1). The NKTZ is considered a part of plate boundary between the NAM and EUR. One important characteristic of the NKTZ is that the high-strain zone is relatively wide, about ~100 km wide. Areas showing maximum contraction strain rates in Central Japan are the Niigata–Northern Fossa magna basin and the region corresponding to the Boso peninsula.

4.3.2 Characteristics of the attenuation maps

Intrinsic absorption. For 1–2 Hz, Q_i^{-1} has the maximum values in Japan reaching $Q_i^{-1} \approx 6.7 \times 10^{-3}$. Strongest attenuation happens in a triangular shaped region that contains the quaternary volcanoes located in the Hida Mountains and Hida highlands in correlation with previous attenuation studies. This region is mainly located in the west side of the ISTL, but its northeast side also contains a portion of the Fossa magna.

In the 2–4 Hz band absorption is strong only in the Northern Fossa Magna also in coincidence with previous studies. For 4–8 Hz the high absorption area is much more reduced. For 8–16 Hz the absorption map looks very similar to the one of 16–32 Hz. The connection between the fore arc region of Tohoku and this wide absorption area is very clear in the 8–16 Hz band. One can observe how the forearc region of northeast Japan ends up in the ISTL. In the western part of this line much stronger attenuation regions can be observed.

In Kanto area, the lowest attenuation appears in the north (also for coda attenuation). This area has high levels of albedo ($B_0 \approx 0.3$) for the 4–8, 8–16 and 16–32 Hz band in this region.

Scattering loss. Q_s^{-1} has high values in the Niigata basin for all frequency bands. In the 1–2 Hz band this region extends up to the Northern Fossa Magna and volcano chain in the Hida range. The Niigata–Northern Fossa magna basin has the highest strain rates of the NKTZ. It also shows high levels of seismic albedo in the 1–2 Hz band. The Boso peninsula and an inland portion of the Izu-Bonin volcanic arc show important values for Q_s^{-1} in the frequency bands for 2–4 and 4–8 Hz. The Boso peninsula shows one of the highest levels of strain rates in Japan. For high frequencies, (4–8, 8–16 and 16–32 Hz) a scattering belt arises at the middle of the ISTL, goes through southern Hida mountains and Hida highlands and continues through the north of Kansai area and Chugoku area. This belt follows the orientation of the active faults contained in it and lies in the southern region of most volcanoes in the west side of the ISTL.

Q_s^{-1} in Tochigi prefecture has values in the first half of the scale for 1–2 and 2–4 Hz, but for 4–8, 8–16 and 16–32 Hz bands the values belong to the second half of the scale. As a consequence, this area shows one of the highest values of albedo in Japan for the 4–8, 8–16 and 16–32 Hz bands.

It is interesting to check the frequency dependence of Q_s^{-1} since the Niigata basin shows up again. Also, around the ISTL a change of behaviour is observed and it seems to behave as a boundary between northeast and southwest Japan. It is notable the

abrupt change in the frequency dependence in the west side of the ISTL.

Attenuation of coda Q_c^{-1} . For the frequency band of 4–8 Hz and higher frequency bands, the low Q_c^{-1} region corresponding to the forearc of northeast Japan seems to end up in the north of Kanto area. These low values for coda attenuation lie inside the region where the PAC has a depth smaller than a 100 km, showing once again the importance of the tectonic setting for the interpretation of our maps.

For 1–2 Hz, stronger attenuation is observed in a quite large triangular region that contains the quaternary volcanoes located in the Hida Mountains and Hida highlands and it is similar to intrinsic attenuation. This region is mainly located in the west side of the ISTL, but its northeast side also contains a small portion of the Fossa magna. This high attenuation region seems to continue in its western side to the north of Kansai area and it reaches Chugoku region. For the same frequency band high attenuation values can be observed in a small region containing volcanoes of the Izu-Bonin volcanic arc. For higher frequencies the maps show significant changes. In the frequency bands of 2–4 Hz, 4–8 Hz and in lesser extent for 8–16 Hz, a high attenuation region can be observed in the northern Fossa magna on the NKTZ. Finally, for 16–32 Hz a wide region with strong attenuation located in the west side of the ISTL is imaged in the map. This area contains the highest number of active faults in Japan.

In Kanto area, the strongest attenuation is observed in the Boso peninsula for 4–8 Hz. This area shows strong contraction rates and strain rates. Although Kanto area is relatively small, it does not show a uniform behaviour and different frequency dependence is observed throughout this region. For instance, the area corresponding to Tochigi prefecture, show a particular frequency dependence and low attenuation for all frequency bands. This region can be also distinguished in the 4–8 Hz map in Jin & Aki (2005).

4.4 Southwestern Japan (Kansai-chugoku-shikoku)

4.4.1 Geological and tectonic setting of southwestern Japan

In the Kansai-Chugoku-Shikoku region the PHS is subducting beneath the EUR from the Nankai Trough with a very shallow dip angle. The Southwestern Japan Arc is divided into an outer (southern) zone and an inner (northern) zone by the MTL (Taira 2001). In the inner zone, mountains, basins and plains are situated complexly as a result of unequal tectonic activities in contrast to the outer zone. Landforms of the Kinki region are characterized by the alternating distribution of north–south oriented mountains and lowlands caused by considerable faults. The Chugoku Mountains extend nearly east to west in the western Kinki region. The Seto Inland Sea, which contains an archipelago, lies between Honshu Island and Shikoku Island. In the outer zone landforms are characterized by mountain belts nearly east–west oriented, the Kii Mountains and the Shikoku Mountains. Shikoku Island and Kii peninsula are under high dilatation, shear and rotational strain rates.

4.4.2 Characteristics of the attenuation maps

Intrinsic absorption. In the 1–2 Hz band, intrinsic absorption show quite uniform values. As we consider higher frequency bands, the lowest values of Q_i^{-1} appears in central Shikoku and north of Chubu and a east–west band of higher attenuation appears between Chugoku and Shikoku that extends to the Kansai area. The highest

values of Q_i^{-1} can be noticed in a spot in the west side of Kii peninsula from 4–8, 8–16 and 16–32 Hz bands. This is the so-called Kinki spot, and has been the subject of numerous studies (Salah *et al.* 2005). In the highest frequency band all Kansai area shows strong intrinsic absorption.

Scattering loss. Shikoku Island and the southernmost region of Kii peninsula show very weak scattering. Shikoku is the area in Japan with the lowest scattering loss for all the frequency bands. Also the seismic albedo shows the lowest values in Japan for Shikoku for all the frequency bands.

In Chugoku, attenuation is slightly higher than in Shikoku for the lowest frequency bands. For the frequency band of 4–8 Hz and for higher frequencies, a strong scattering/high albedo area arises in Chugoku, probably related with the arc of Quaternary volcanoes located near the shore of the Japan sea, since this high scattering region continues to the north of Kansai and reaches the region of quaternary volcanoes in Chubu area. For 4–8 Hz and higher frequency bands also a strong scattering region (the Kinki spot) in the west side of the Kii peninsula can be seen.

Coda Q_c^{-1} . For 1–2 Hz the quaternary volcanic arc of Honshu becomes visible as a high attenuation band from western Chugoku to the centre of Japan in the Chubu region. Values of attenuation are quite low for Shikoku and also the north of Chugoku area for higher frequency bands. In Kansai, the Kinki spot can be seen in the west side of Kii peninsula for all frequency bands with different degrees of attenuation for each frequency band. This spot is not detected in Jin & Aki (2002), but, in general, a higher similarity is found with our maps in this area of Japan for 2–4, 4–8 and 8–16 Hz.

4.5 Kyushu

4.5.1 Geological and tectonic setting of Kyushu

Kyushu island is located at the intersection of the southwestern Honshu arc and the Ryukyu arc. Very active volcanoes are located in this island: Unzen, Aso, Sakurajima, etc. The Unzen volcano is located at the western tip of the central Kyushu Rift Valley or Beppu-Shimabara Graben, which divides Kyushu into northern and southern blocks. The Northern area of Kyushu Island is the extension of the inner zone of the Chugoku region. Some of the geomorphic characteristics and the nature of past volcanic activities are similar to those of the Korean Peninsula (Taira 2001). A non volcanic mountain belt, the Kyushu Mountains, is located to the south of the volcanic zone of central Kyushu. Active volcanoes are distributed along the volcanic front of the Ryukyu Arc to the south of the Kyushu Mountains. At Kagoshima Bay, the Sakurajima Volcano is the most active volcano in Japan, situated in the southern end of Kyushu. Sakurajima volcano accumulates a high dilation rate. Contractual strains are important in the eastern part of the central area. Large shear strain rates are observed in the southern area as well as rotational strain rates.

4.5.2 Characteristics of the attenuation maps

Intrinsic absorption. In the 1–2 Hz band, strong absorption happens in a region populated by the Quaternary volcanoes on the west side of the Beppu-Shimabara grabben. Q_i^{-1} shows clearly lower values for the north region in the 2–4, 4–8 and 8–16 Hz bands. The northern region behaves then as an extension of Chugoku area for these frequency bands. The central and southern region show higher values in correlation with the existence of the volcanic arcs.

It is notable the difference between these areas and the behaviour of the areas of Chugoku and Shikoku for the 2–4 and 4–8 Hz frequency bands. Q_i^{-1} shows strong values in a region approximately corresponding to the Kyushu mountains for the frequency bands of 8–16 and 16–32 Hz.

Scattering loss. Q_s^{-1} has large values only in the volcanic region corresponding to the central and eastern part of the Beppu Shimabara graben for all the frequency bands. This volcanic region contains important volcanoes: the volcanoes Aso, Kuju, Yufu and Tsurumi around Kujyu Volcano Group. Seismic albedo also shows important values in this area for 1–2 Hz mainly north and southern areas take smaller values than central area. For the other frequency bands, intrinsic absorption is the main mechanism for the attenuation of coda waves.

Attenuation of coda Q_c^{-1} . Q_c^{-1} follows a behaviour similar to intrinsic absorption, showing a different behaviour for the northern area and for the central and southern area, which shows high attenuation values in clear relation with the volcanic arcs. However, for the other frequency bands, highest attenuation mainly concentrates in the volcanic areas in central and southern Kyushu. In Jin & Aki (2005) they found mainly high attenuation in the 2–4 Hz band in the central part of the Beppu Shimabara Grabben.

5 DISCUSSION

In the last section, we have shown maps of the seismic wave attenuation parameters which show strong regional variation of the parameters. We discuss now the possible relationship of the results with the geotectonic setting of each region, volcanism mechanisms, and velocity structure obtained by means of seismic tomography.

Wang & Zhao (2005) determined detailed 3-D seismic velocity structures in Hokkaido. They found strong low velocity zones in the crust and upper mantle wedge continuously along the NE Japan and Kuril arcs beneath the active volcanoes. They consider that these anomalies are caused by large volumes of aqueous fluids that are released from the subducting slab. Also in the north region of Hokkaido island at shallow depths it shows very low velocity for both V_p and V_s and high V_p/V_s ratio (Nakamura *et al.* 2008). This large anomaly seems to extend towards the south and ends up in the west side of Hidaka Mountains. The results in our maps strongly correlate with these results. We obtain high scattering or/and strong absorption in these areas. The frequency dependence of scattering can be interpreted in terms of the size of the heterogeneities caused by the upflow of fluids and the frequency dependence of absorption probably depends on the composition and distribution of the fluids. Clearly, the strong absorption in the northern region might be related with the presence of partially melted magma at shallow depths.

In the Tohoku area, the different level of intrinsic absorption between the backarc and forearc that shows up in our maps has already been reported by several authors using quite different methods. For example, (Tsumura *et al.* 1996, 2000) found low Q_p^{-1} values are distributed in the Kitakami and Abukuma mountain ranges and high Q_p^{-1} zones are distributed along the volcanic front to the west of these mountain ranges. In Yoshimoto *et al.* (2006) and in the citations there in a stronger absorption of seismic waves is found in the volcanic range and the west side of it. In Sekine (2005) it is also possible to clearly observe a higher attenuation in the volcanic range and its west side in the 5 Hz band. Similar results were obtained earlier by Umino & Hasegawa (1984).

Wang & Zhao, (2005) observe very clearly that the velocity anomalies are located under the volcanoes and report low-velocity

zones in the uppermost mantle beneath the volcanic front, which are inclined towards the backarc side. This is also nicely depicted in fig. 12 of Nakajima *et al.* (2001). They believe that large volumes of aqueous fluids might be released upwards by dehydration reactions in the subducting oceanic crust and sediments. This uneven distribution of the velocity anomalies together with a corresponding higher level of fluid uploading may, in our opinion, be the origin of the different amount of absorption that we observe in the backarc region. Moreover, the velocity anomalies are able to scatter seismic waves. Studying the peak delay analysis of *S*-wave envelopes, Takahashi *et al.* (2007) found that peak delay times observed in the backarc side of the volcanic front show clear path dependence related to the Quaternary volcano distribution. Only large peak delays were observed for the ray paths propagating beneath Quaternary volcanoes. This means that seismic waves suffer multiple forward scattering and diffraction during their traveltime inside the low velocity structures.

The strongest low velocity anomaly in the fore arc happens under the area corresponding to the Sendai plain, at quite shallow depths (Wang & Zhao 2005). They detected it from 25 to 40 km. Also, in the same area, in the cross sections of velocity anomalies for *P* and *S* waves in Nakajima *et al.* (2001), it is possible to observe a low velocity anomaly for *P* and *S* waves with a high V_p/V_s ratio that seems a prolongation of a more deeper v-shaped body that seems to feed the volcanic range. This region has been the subject of a deeper analysis in Asano *et al.* (2004). They computed a 3-D distribution of scattering coefficients in this area. They report large scattering zones in this area that merge in the lower crust. These regions also correlate with the known low velocity regions. Then this low velocity anomaly/high scattering area together with its deeper structure is related with the strong scattering attenuation in our scattering maps for all the frequency bands.

In central Japan, it seems quite clear the relationship between the shape of our maps and the volcanism and tectonic setting of this complex area. For instance, Nakajima & Hasegawa (2007) clearly show the existence of low velocity areas under the volcanoes of central Japan. These low velocity areas are interpreted as the upflow of partially melted magma and water from the dehydration of the subducting Philippine sea slab and they probably feed the volcanic area. The PAC, which lies underneath the PHS in the west side of the ISTL, does not produce volcanism in this area, since the upflow from the PAC is blocked by the PHS. It is quite surprising that the scattering belt in our maps stops suddenly at the ISTL. However in the north of Central Japan, may be the upwelling from the PHS helps creating a continuous volcanic arc that shows high levels of absorption and/or scattering.

In several frequency bands, a high attenuation region can be observed in the northern Fossa magna, especially for Q_i^{-1} and Q_c^{-1} . This strong attenuation region coincides with the one studied by Kurashimo & Hirata (2004) and Sato *et al.* (2004). They found a low velocity zone and low V_p/V_s , that extends to a depth of 10 km which indicated the presence of aqueous fluid filled pores. Although they did not determine the extent of this region, it seems from our maps that it corresponds to a large area in the Fossa Magna. This region extends in south direction through the ISTL tectonic line up to approximately to its coincidence with the MTL. This region contains an important number of quaternary volcanoes from both sides of the ISTL. In the north direction it seems to extend to the Niigata Basin.

In the northern area of Kanto region, in the area of Tochigui prefecture, the velocity of *S*-waves is the lowest in Japan for shallow depths ≤ 5 km (Matsubara *et al.* 2008). For 10 km depth, however,

the reported velocity anomaly for *V_s* turns to positive values. For 20–30 km depth, high V_p/V_s values are reported in the west side of the prefecture in a region under active quaternary volcanoes. In this area, the resulting intrinsic attenuation is low, scattering is relatively high and as a consequence albedo is so high. May be some trapping of energy happens because of the velocity contrast at shallow depths, producing a low attenuation of the seismic waves.

It is interesting to compare the frequency dependence of Q_c^{-1} in relation with the volcanic front and the strong frequency dependence of envelope broadening observed in the forearc region by Obara & Sato (1995). In the west of the volcanic front, scattering loss decreases with frequency faster than in the east side. Obara & Sato (1995) found a very similar result; the frequency dependence of envelope broadening is also higher in west side of the volcanic front.

The NKTZ does not show up as a uniform tectonic line, as for instance, the ISTL. In the 1–2 Hz band, for the maps of seismic albedo and scattering loss, the ISTL seems clearly a sharp boundary between Northeast Japan and Southwest Japan. However, remarkable facts can be noticed on the NKTZ for different frequency bands and attenuation parameters. Its northern side shows high scattering loss for all frequency bands. In the central part high absorption values can be noted for the 1–2 Hz band. In its southern part in Kansai region, high scattering values can be observed for 4–8, 8–16 and 16–32 Hz. For Q_c^{-1} very important attenuation is observed in the 1–2 Hz in the southern and central regions and for 2–4 Hz in the northern region. In Jin & Aki (2005) they found higher attenuation in the northern and central part of the NKTZ for the 1–2 Hz band. Finally, we would like to note that attenuation is not produced by high-stress ratios, but it may be produced by some of its consequences. However, higher correlation between low velocity anomalies on the NKTZ and the corresponding values of the attenuation parameters has been established.

In a recent paper, tomographic evidence for the mantle upwelling in southwestern Japan has been reported (Nakajima & Hasegawa 2007). Their results show the existence of a large low-velocity anomaly below the Philippine sea slab in the Chugoku and Shikoku districts at least down to depths of 300 km. From this deep low velocity zone, two shallower low-velocities are detected. One is located in the Chugoku area, in the leading edge of the PHS. The leading edge is located under the Chugoku Mountains and has been detected by means of velocity tomography (Nakajima & Hasegawa 2007) and previously from receiver function analysis (Shiomi *et al.* 2004). It extends to the north of Kansai area and reaches the volcanic area in the centre of Chubu region. The low velocity zones are interpreted as upwelling of magma flow that feeds the quaternary volcanoes in the north of Chugoku area. We would like to notice also that the Moho and the Conrad discontinuities bends down just beneath the Chugoku mountains (Yamauchi *et al.* 2003; Shiomi *et al.* 2004) probably in relation with the velocity anomaly.

In Kii peninsula, the upwelling happens through the slab at depths of 30–60 km beneath the Kii peninsula in the Kinki spot. It has been studied previously by several authors, and their results correlate with this interpretation: high terrestrial heat flow is detected in the western part of Kii peninsula (Okubo 1993). Also (Salah *et al.* 2005) and Nakamura *et al.* (2008) report low values for *V_s* and V_p in western Kii peninsula. (Salah & Zhao 2003) interpreted previously the shallow low velocity region as produced by fluids coming from the dehydration of the subducting Philippine Sea slab and show rather clear velocity maps although only for shallow depths for this velocity anomaly. Then, the correlation with the results in our maps

for scattering loss is quite clear. The high scattering regions clearly coincides with both low velocity regions both in size and extent. The frequency dependence in scattering can then be interpreted in terms of the scale of the heterogeneities in every region. Scattering coefficients show then a different behaviour for the inner and forearc for the higher frequencies.

The PHS subducts very steeply under Kyushu down to depths of 150–200 km. It is the steepest subduction geometry in Japan (Nakajima & Hasegawa 2007). The differences in the slab geometry between the adjacent regions of Chugoku and Shikoku correlate with the differences in our maps, as well as volcanic activity, suggesting the importance of the geometry of the PHS on the properties of the crust. In the south of Kyushu, prominent low-velocity anomalies are visible at depths of 10–40 km along the upper boundary of the subducting plate (Wang & Zhao 2006; Nakajima & Hasegawa 2007; Nakamura *et al.* 2008; Matsubara *et al.* 2008). This volume may correspond to the upwelling flow from the dehydration of the slab. Then, it seems possible to correlate the high absorption levels in Kyushu to the existence of magma flow that originates the volcanism in Kyushu. For example, in Wang & Zhao (2006), it is possible to observe, in the figures corresponding to vertical sections, two large velocity anomalies from a depth of 60 km up to the surface under the central part and northeast part of the Kyushu Mountains, although in those areas there are no volcanoes. In the frequency band of 8–16 Hz, the maximum values of Q_i^{-1} corresponds to those areas.

6 FURTHER DISCUSSION AND CONCLUSIONS

High resolution maps of the seismic wave attenuation parameters (scattering loss and intrinsic absorption) have been obtained by using the MLTWA with *S*-wave data in high frequencies (1–32 Hz range) provided by the Hi-net seismic network. The maps show strong regional variation of the parameters. We have shown that these variations are related mainly with the geotectonic setting of each region and its volcanism mechanisms. For the lower frequency bands, it is possible to identify volcanic areas of Japan because they show strong scattering loss and/or strong intrinsic absorption. For higher frequency bands there are also high scattering and/or absorption regions that correlate with the existence of low velocity anomalies that are interpreted by other authors as upflow of partially melted magma and water from the dehydration of the subducting PAC and PHS. Then our results match well with the data obtained by means of seismic tomography. Certainly, scattering is mainly produced by velocity and density fluctuations of the media. Velocity fluctuations are expected to be higher in low velocity regions, where fluids like partially melted magma and/or water accumulates or flow. Examples of this kind of region are the volcanic regions. In the volcanic regions seismic waves are known to be strongly scattered (Carcole *et al.* 2006). Moreover, intrinsic absorption is strongly correlated with the presence of fluids.

Also some correlation has been observed with strain analysis in Japan. Some areas showing high strain ratios show also strong scattering or absorption values. However, this factor by itself does not seem to be enough to explain the local variations of the parameters, since some regions accumulating high strain ratios do not show any particular behaviour, like Shikoku region. Also, some correlation with stress analysis can be found in the maps showing frequency dependence. The higher exponents correspond to regions with high stress, like the NKTZ. However there are again regions like Shikoku

that accumulates high dilatation, shear and rotation rates, but show no distinctive behaviour.

The MLTWA is based on the hypothesis of multiple isotropic scattering in a medium with the homogeneous distribution of scattering coefficient and intrinsic absorption. Although these hypothesis are too simple in the crust of Japan because of the depth dependence and lateral variations on the parameters as, for instance, the velocity of the propagation of the seismic waves, the results are very informative on the characteristics of each region and show the usefulness of the study of the properties of scattered seismic waves in the understanding of the properties of the crust.

The frequency dependence of the parameters is related with the spectral structure of medium heterogeneity. The spectral structure of the media may imply that scattering is not isotropic phenomenon, but highly anisotropic and depending on frequency. Neglecting anisotropic scattering may bias the measurements of the scattering loss. Then, further mathematical development that may allow using anisotropic scattering theories (Sato & Fehler 1998; Carcole & Ugalde 2008) should be necessary in order to get a better measurement of the scattering parameters.

In media with anisotropic scattering one may infer that the MLTWA provides an estimate of an effective scattering loss parameter which is not proportional to the scattering mean free path but to the transport mean free path. In fact, Abubakirov (2005) established a quantitative measure of the biasing of the scattering parameters when the MLTWA method is used. By taking into account the numerical simulations performed in Gusev & Abubakirov (1996) by means of the Monte Carlo method, it is possible to conclude that the MLTWA provides an estimate of about one half of the effective scattering loss coefficient (proportional to the inverse of the transport mean free path), defined by $Q_e^{-1} = Q_{ani}^{-1} (1 - \langle \cos \theta \rangle)$ where Q_{ani}^{-1} is proportional to the inverse of the scattering mean free path due to the anisotropic scattering and $\langle \cos \theta \rangle$ is the average cosine of the scattering angle. This quantitative statement is valid for media with Gaussian or fractal power spectral density and moderate forward scattering.

In addition, the vertical stratification of both scattering loss and intrinsic absorption is another fact that may introduce a bias in the results. It has been established by Wegler (2004) that the existence of velocity and/or vertical stratification of the properties of the media have an impact on the estimate of intrinsic absorption. Leakage of energy under volcanoes leads to an apparent exponential decay of the coda which cannot be interpreted as intrinsic attenuation. In the Japanese islands, there is not only vertical stratification but also a non-negligible lateral dependence of the parameters. As already pointed out, these lateral variations are due to the existence of subducting slabs through the east coast, the existence of volcanic arcs through the islands and the existence of low velocity anomalies. These strong lateral inhomogeneities become even clearer when the 3-D velocity model necessary to describe the propagation of both *P* and *S* waves in Japan is depicted. Perhaps it might be possible in future studies to develop a model for the better estimation of the parameters by taking into account the complex lateral and vertical structure of the Japanese islands.

ACKNOWLEDGMENTS

We are grateful to those who make efforts to run the Hi-net and data provided by NIED staff in Tsukuba, Japan and in particular with Kazushige Obara and Takuto Maeda. We are grateful with Junichi Nakajima for useful discussions. Eduard Carcole is now enjoying a fellowship of Global COE program for Earth Science in Tohoku

University, Sendai, Japan. This work started during a 6 months stay under a 'Juan de la Cierva' contract and a 'Jose Castillejo' grant of the Spanish Ministerio de Ciencia y Tecnologia (MCYT). This research has been partially supported by the MCYT projects CGL-2005-04541-C03-02/BTE and CGL2008-00869/BTE. Seismic Analysis Code (SAC) and GMT code are used for data processing and figure plotting. This work has used 'Active Fault Shape File' from Nakata, T. and Imaizumi, T., eds, 2002, 'Digital Active Fault of Japan', University of Tokyo Press (product serial number: DAFM0544). We acknowledge the help provided by Mare Yamamoto in the use of GMT routines and helpful hints in the elaboration of computer programs to manage Hi-net data. We also acknowledge the help of Hirotooshi Nishiwaki in the elaboration of Fig. 2. The authors are also grateful to the comments of the editor Mike Kendall and two anonymous reviewers that further improved this paper.

REFERENCES

- Abubakirov, I.R., 2005. Attenuation characteristics of transverse waves in the lithosphere of Kamchatka estimated from observations at the Petropavlovsk digital broadband station, *Izvestiya-Phys. Solid Earth*, **41**, 813–824.
- Aki, K., 1980. Attenuation of shear waves in the lithosphere for frequencies from 0.05 to 25 Hz, *Phys. Earth planet. Inter.*, **21**, 50–60.
- Aoyama, H., Takeo, M. & Ide, S., 2002. Evolution mechanisms of an earthquake swarm under the Hida Mountains, central Japan, in 1998, *J. geophys. Res.-Solid Earth*, **107**, 2174.
- Arita, K. *et al.*, 1998. Crustal structure and tectonics of the Hidaka collision zone, Hokkaido (Japan), revealed by vibroseismic reflection and gravity surveys, *Tectonophysics*, **290**, 197–210.
- Asano, Y. *et al.*, 2004. Inhomogeneous crustal structure beneath northern Miyagi prefecture, northeastern Japan, imaged by coda envelope inversion: implication for fluid distribution, *Geophys. Res. Lett.*, **24**, L24615.
- Carcole, E. & Ugalde, A., 2008. Formulation of the multiple anisotropic scattering process in two dimensions for anisotropic source radiation, *Geophys. J. Int.*, **174**, 1037–1051.
- Carcole, E., Ugalde, A. & Vargas, C.A., 2006. Three-dimensional spatial distribution of scatterers in Galeras volcano, Colombia, *Geophys. Res. Lett.*, **33**, L08307.
- Fehler, M. *et al.*, 1992. Separation of scattering and intrinsic attenuation for the Kanto-Tokai region, Japan, using measurements of s-wave energy versus hypocentral distance, *Geophys. J. Int.*, **108**, 787–800.
- Fukao, Y. & Yamaoka, K., 1983. Stress estimate for the highest mountain system in Japan, *Tectonics*, **2**, 453–471.
- Gusev, A.A. & Abubakirov, I.R., 1996. Simulated envelopes of non-isotropically scattered body waves as compared to observed ones: another manifestation of fractal heterogeneity, *Geophys. J. Int.*, **127**, 49–60.
- Hasegawa, A. *et al.*, 2005. Deep structure of the northeastern Japan arc and its implications for crustal deformation and shallow seismic activity, *Tectonophysics*, **403**, 59–75.
- Hashimoto, C. & Matsu'ura M., 2006. 3-D simulation of tectonic loading at convergent plate boundary zones: internal stress fields in Northeast Japan, *Pure appl. Geophys.*, **163**, 1803–1817.
- Hoshiha, M., 1991. Simulation of multiple-scattered coda wave excitation based on the energy-conservation law, *Phys. Earth planet. Inter.*, **67**, 123–136.
- Hoshiha, M., 1993. Separation of scattering attenuation and intrinsic absorption in Japan using the multiple lapse time window analysis of full seismogram envelope, *J. geophys. Res.-Solid Earth*, **98**, 15 809–15 824.
- Hoshiha, M. & Goto, K., 1988. Regionality of seismic wave attenuation in Japan (in Japanese), *Prog. Abstr. Seismol. Soc. Jpn.*, **1**, B01.
- Itoh, Y., Ishiyama, T. & Nagasaki, Y., 2005. Deformation mode in the frontal edge of an arc-arc collision zone: subsurface geology, active faults and paleomagnetism in southern central Hokkaido, Japan, *Tectonophysics*, **395**, 81–97.
- Jin, A. & Aki, K., 2005. High-resolution maps of Coda Q in Japan and their interpretation by the brittle-ductile interaction hypothesis, *Earth Planets Space*, **57**, 403–409.
- Kato, M., Katsui, Y., Kitagawa, Y. & Matsui, M., 1990. *Regional Geology of Japan: Part 1. Hokkaido*, Kyoritsu, Shuppan, Tokyo.
- Katsumata, K., Urabe, T. & Mizoue, M., 1995. Evidence for a seismic attenuation anomaly beneath the Hida Mountain Range, Central Honshu, Japan, *Geophys. J. Int.*, **120**, 237–246.
- Kosuga, M., 1992. Dependence of Coda-Q on frequency and lapse time in the western Nagano Region, Central Japan, *J. Phys. Earth*, **40**, 421–445.
- Kurashimo, E. & Hirata, N., 2004. Low Vp and Vp/Vs zone beneath the northern Fossa Magna basin, central Japan, derived from a dense array observation, *Earth Planets Space*, **56**, 1301–1308.
- Lindquist, K.G., Engle, K., Stahlke, D. & Price, E., 2004. Global Topography and Bathymetry Grid Improves Research Efforts, *EOS, Trans. Am. Geophys. Un.*, **85**(19), 186.
- Nakajima, J. & Hasegawa, A., 2007. Subduction of the Philippine sea plate beneath southwestern Japan: Slab geometry and its relationship to arc magmatism, *J. geophys. Res.*, **112**, B08306.
- Nakajima, J. *et al.*, 2001a. Seismic imaging of arc magma and fluids under the central part of northeastern Japan, *Tectonophysics*, **341**, 1–17.
- Nakajima, J. *et al.*, 2001b. Three-dimensional structure of V-p, V-s, and V-p/V-s beneath northeastern Japan: implications for arc magmatism and fluids, *J. geophys. Res.-Solid Earth*, **106**, 21 843–21 857.
- Nakamura, R. *et al.*, 2006. Three-dimensional attenuation (Qs) structure beneath the Kanto district, Japan, as inferred from strong motion records, *Geophys. Res. Lett.*, **33**, L21304.
- Nakamura, M. *et al.*, 2008. Three dimensional P- and S-wave velocity structures beneath Japan, *Phys. Earth planet. Inter.*, **168**, 49–70.
- Nakata, T. & Imaizumi, T., 2002. *Digital Active Fault of Japan*, University of Tokyo Press.
- Matsubara, M., Hirata, N. & Saka, S., 2000. A low velocity zone beneath the Hida Mountains derived from dense array observation and tomographic method, *Earth Planets Space*, **52**, 143–154.
- Matsubara, M., Obara, K. & Kasahara, K., 2008. "Three-dimensional P- and S-wave velocity structures beneath the Japan Islands obtained by high-density seismic stations by seismic tomography", *Tectonophysics*, **454**, 86–103.
- Mizoue, M., Haneda, T., Hashimoto, S., Nakamura, I., Katsumata, A. & Yokota, T., 1983. Anomalous seismic attenuation beneath the Hida Mountain Range, *Abstract for the Annual Meeting of the Seismological Society of Japan*, **2**, 198.
- Obara, K. & Sato, H., 1995. Regional differences of random inhomogeneities around the volcanic front in the Kanto-Tokai area, Japan, revealed from the broadening of S-wave seismogram envelopes, *J. geophys. Res.-Solid Earth*, **100**(B2), 2103–2121.
- Obara, K., Kasahara, K., Hori, S. & Okada, Y., 2005. A densely distributed high-sensitivity seismograph network in Japan: Hi-net by National Research Institute for Earth Science and Disaster Prevention, *Rev. Scient. Instrum.*, **76**, 021301.
- Okada, Y. *et al.*, 2004. Recent progress of seismic observation networks in Japan: Hi-net, F-net, K-NET and KiK-net, *Earth planet. Science*, **56**, 15–28.
- Okubo, Y., 1993. Temperature gradient map of the Japanese Islands. *J. Geother. Res. Soc. Japan*, **15**, 1–21.
- Paasschens, J.C.J., 1997. Solution of the time-dependent Boltzmann equation, *Phys. Rev. E*, **56**, 1135–1141.
- Salah, M.K. & Zhao, D.P., 2003. Seismic structure of Kii Peninsula in southwest Japan: evidence for slab dehydration in the forearc, *Tectonophysics*, **364**, 191–213.
- Salah, M.K., Zhao, D.P., Lei, J.S. & Abdelwahed, M.F., 2005. Crustal heterogeneity beneath southwest Japan estimated from direct and Moho-reflected waves, *Tectonophysics*, **395**, 1–17.

Q14

Q15

Q16

Q17

Q18

Q19

Q20

Q21

- Sagiya, T., Miyazaki, S. & Tada, T., 2000. Continuous GPS array and present-day crustal deformation of Japan, *Pageoph*, **157**, 2303–2322.
- Sato, H., 1994. The relationship between late Cenozoic tectonic events and stress-field and basin development in northeast Japan, *J. geophys. Res.-Solid Earth*, **99**, 22 261–22 274.
- Sato, H. & Fehler, M.C., 1998. *Seismic Wave Propagation and Scattering in the Heterogeneous Earth*, AIP Series in Modern Acoustics and Signal Processing, Springer-Verlag, New York.
- Sato, H. *et al.*, 2004. Seismological and geological characterization of the crust in the southern part of northern Fossa Magna, central Japan, *Earth Planets Space*, **56**, 1253–1259.
- Q22 Sekine, S., 2005. Tomographic inversion of ground motion amplitudes for the 3-D Attenuation Structure beneath the Japanese Islands, *Report of the National Research Institute for Earth Science and Disaster Prevention*, **68**, 137–173.
- Shiomi, K., Sato, H., Obara, K. *et al.*, 2004. Configuration of subducting Philippine Sea plate beneath southwest Japan revealed from receiver function analysis based on the multivariate autoregressive model, *J. Geophys. Res.-Solid Earth*, **109**, B04308.
- Tada, T., Sagiya, T. & Miyazaki, S., 1997. The Deforming Japanese Islands as Viewed with GPS, *Kagaku*, **67**, 917–927 (in Japanese).
- Taira, A., 2001. Tectonic evolution of the Japanese island arc system, *Annu. Rev. Earth planet. Sci.*, **29**, 109–134.
- Takahashi, T. *et al.*, 2007. Strong inhomogeneity beneath Quaternary volcanoes revealed from the peak delay analysis of S-wave seismograms of microearthquakes in northeastern Japan. *Geophys. J. Int.*, **168**, 90–99.
- Q23 Toya, Y. & Kasahara, M., 2005. M Robust and exploratory analysis of active mesoscale tectonic zones in Japan utilizing the nationwide GPS array, *Tectonophysics*, **400**, 27–53.
- Tsumura, N., Hasegawa, A. & Horiuchi, S., 1996. Simultaneous estimation of attenuation structure, source parameters and site response spectra - application to the northeastern part of Honshu, Japan, *Phys. Earth planet. Inter.*, **93**, 105–121.
- Tsumura, N. *et al.*, 2000. Three-dimensional attenuation structure beneath the northeastern Japan arc estimated from spectra of small earthquakes, *Tectonophysics*, **319**, 241–260.
- Q24 Umino, N. & Hasegawa, A., 1984. Three dimensional Qs structure in the Northeastern Japan arc, *Zisin (in Japanese)*, **37**, 217–228.
- Ueda, H., 2005. Accretion and exhumation structures formed by deeply subducted seamounts in the Kamuikotan high-pressure/temperature zone, Hokkaido, Japan, *Tectonics*, **24**, TC2007.
- Q25 Wegler, U., 2004. Diffusion of seismic waves in a thick layer: theory and application to Vesuvius volcano, *J. geophys. Res.*, **109**, B07303, doi:10.1029/2004JB003048.
- Yamada, N., Nozawa, T., Harayama, S., Takizawa, F., Kato, H., Hiroshima, T. & Komazawa, M., 1989. *Geological sheet map 1:200,000 Takayama*, Geol. Surv. Jpn. Geol. Map, NJ-53–6.
- Yamazaki, F., 1996. A wall-like low-Q zone beneath the Yakedake Volcano, central Japan. *J. Phys. Earth*, **44**, 23–38.
- Yoshimoto, K. & Jin, A., 2008. Coda energy distribution and attenuation, *Adv. Geophys.*, **50**, 265–299.
- Yoshimoto, K., Wegler, U. & Korn, A., 2006. A volcanic front as a boundary of seismic-attenuation structures in northeastern Honshu, Japan, *Bull. seism. Soc. Am.*, **96**, 637–646.
- Yamauchi, M., Hirahara, K. & Shibutani, T., 2003. High resolution receiver function imaging of the seismic velocity discontinuities in the crust and the uppermost mantle beneath southwest Japan, *Earth Planets Space*, **55**, 59–64.
- Wang, Z. & Zhao, D.P., 2005. Seismic imaging of the entire arc of Tohoku and Hokkaido in Japan using P-wave, S-wave and sP depth-phase data, *Phys. Earth planet. Inter.*, **152**, 144–162.
- Wang, Z. & Zhao, D.P., 2006. Vp and Vs tomography of Kyushu, Japan: New insight into arc magmatism and forearc seismotectonics, *Phys. Earth planet. Inter.*, **157**(3–4), 269–285.
- Q26 William, H. *et al.*, 2007. *Numerical Recipes: The Art of Scientific Computing*, 3rd edn, Cambridge University Press.

- Zeng, Y.H., Su, F. & Aki, K., 1991. Scattering wave energy propagation in a random isotropic scattering medium. 1: theory., *J. geophys. Res.-Solid Earth Planets*, **96**, 607–619.

APPENDIX A: SOME TECHNICAL DETAILS OF THE MAPPING PROCESS WITH GMT

Mapping the results has been performed by means of GMT routines. It is important to provide a small description of technical details of GMT routines in order to allow readers to reproduce the maps and understand our mapping procedure. The function ‘blockmean’ has been used to create a grid with a spacing of 0.04° (about 4.5 km) from the original data (which contains only the coordinates of each station and the value of a parameter). This grid distance is used for all the functions here commented and it is smaller than the distance between stations. Then, we make sure that each station only contributes to a single gridpoint located very near to the station. The function surface is used to generate a continuous map with a ‘tension factor’ of 1.0, which is the maximum value. This value makes it possible to show strong local gradients in the maps when they are present. Then, in a few particular cases, values of single stations can be seen as spots of a different colour. We note here that the function surface interpolates the value of a parameter between the stations in order to assign a value to each point of the grid. In this way a continuous distribution may be shown in the maps. The function *grdmask* is used with a radius of 0.25°; then, the map shows no results if there is no information from any station inside this radius for each gridpoint. This choice limits the maximum interpolation distance in the map. In conclusion, the values of the parameters have been decided as a trade-off between trying to show an informative continuous distribution and at the same time trying to keep the maximum original information about local variations of the parameters being measured.

In order to make clear the importance of the results for every region, a special colour palette has been used to perform each map as in (Carcole *et al.* 2006). This colour palette has 14 colours. This allows identifying regions with similar or constant values of the parameters, and at the same time allows observing important gradients when they are present. The maximum and minimum values of the map correspond to maximum and minimum values of the parameters; this allows visualizing clearly the different behaviour of each region.

APPENDIX B: COMPARISON BETWEEN HOSHIBA (1993) AND THE RESULTS IN THIS PAPER. ERROR MAPS

In order to show consistency with previous results, we perform a comparison between Hoshiba (1993) and our results obtained with Hi-net data. Hoshiba (1993) is the only source that allows us comparing all the parameters calculated by means of a very similar analysis in different regions of Japan. The comparison has been done for the three frequency bands between the 16 stations used in Hoshiba’s paper and the interpolated results plotted in our maps. Comparison is easy since he explicitly wrote down his results in a table. Comparison is shown in Tables B1–B3. Taking into account that the data set is different, that he used a constant velocity model, that he analysed each component separately and that we are interpolating results with nearby stations, the correlation with our results

Table B1. Comparison with Hoshiba's results (1993) for frequency band 1–2 Hz.

Station	Q_c^{-1} (1)	Q_c^{-1} (2)	Q_s^{-1} (1)	Q_s^{-1} (2)	Q_i^{-1} (1)	Q_i^{-1} (2)
KAGOS2	4.9	5	3.2	3.5	6.2	5.2
KUMAM2	7.2	7.5	5	5.3	6.9	6.5
SHIMO2	4.5	4.3	5.6(−4.1)	2.8	7.1(−3.9)	5.1
YONAG2	4.9	6.2	1.9(+1.8)	4.0(−1.8)	3.2(+2.5)	5.2
TOKUS2	5.4	5.7	1.53(+0.4)	2.2(−1.1)	4.8	5.4
WAKAY2	6.7	6.7	1.66(+2.2)	4.0(−1.4)	3.9(+2.2)	5.7(−1.4)
TSURU2	5.9	6.7	4.4	4.2	6.6	5.8
CHICH2	6.3	6.1	5.7	5.3	5.3	5.1
MATSU2	10	7.8	14.5(−1.9)	8.0(+2.5)	10.5(−0.3)	6.5(+1.3)
KAKIO2	4.3	4.9	4	4.4	3.7	4.7
NIIGA2	5.3	4.8	1.77(+3.4)	8.3(−1.6)	5	4.1
YAMAG2	4.6	6.3	13.3(−4.1)	6.5(+2.8)	6.2	5.8
OFUNA2	3.7	4.2	3.9	3.2	5.9(−1.8)	4.5
AOMOR2	4.8	4.6	2.9(+3.9)	5.8	1.36(+3.1)	4
HIROO2	4.9	4.2	4.3	4.4	4.6	4.6
KUSHI2	3.6	3.2	6.2(−2.1)	5.3	4.9(−1.4)	3(+1.26)

Notes: Hoshiba's results are indicated by (1) and ours by (2). Discrepancies are indicated by bold numbers. The criterion for discrepancy is that the result from Hoshiba does not match our result inside error bounds. We provide error bounds between brackets when necessary. For Q^{-1} we considered that there is a discrepancy for differences higher than 25 per cent.

Table B2. Comparison with Hoshiba's results (1993) for frequency band 2–4 Hz.

Station	Q_c^{-1} (1)	Q_c^{-1} (2)	Q_s^{-1} (1)	Q_s^{-1} (2)	Q_i^{-1} (1)	Q_i^{-1} (2)
KAGOS2	4.2	4.9	1.7(−0.9)	1.1	4.9	4.7
KUMAM2	4.2	4.7	1.17	1.2	3.7(+0.5)	4.3(−0.86)
SHIMO2	2.7	2.8	1.02	0.95	2.4(+0.5)	3.4(−0.81)
YONAG2	2.6	3.3	0.72(+0.58)	1.17	2(+1.1)	2.9
TOKUS2	3	3.1	0.36(+0.09)	0.7(−0.3)	2.6(+0.3)	3.1(−0.7)
WAKAY2	4.2	4.2	0.58(+0.23)	1.0(−0.37)	3(+0.5)	3.8(−0.68)
TSURU2	2.9	3.8	0.81(+0.36)	1.1	3.2	3.3
CHICH2	3.3	3.5	1.94(−0.86)	1.3(+0.6)	3.2	3.5
MATSU2	5.8	5.4	3.1(−1.4)	1.5	5.6(−1.6)	4.7
KAKIO2	2.9	3.5	1.53	1.5	2.7(+1.1)	3.7
NIIGA2	3.6	4.9	0.98(+0.92)	1.5	3.9	4.1
YAMAG2	2.2	4.2	0.77(+0.25)	1.3(−0.6)	2(+0.4)	4.1(−1)
OFUNA2	2.4	2.7	0.99	1	2.8	2.9
AOMOR2	3.4	4.2	1.44	1.6	2.8(+0.9)	4.1(−0.9)
HIROO2	2.9	3.3	1.91(−0.76)	1.2	3.4	3.6
KUSHI2	2.8	2.9	1.76(−0.74)	1.5	3.1	3.1

Notes: Hoshiba's results are indicated by (1) and ours by (2). Discrepancies are indicated by bold numbers. The criterion for discrepancy is that the result from Hoshiba does not match our result inside error bounds. We provide error bounds between brackets when necessary. For Q^{-1} we considered that there is a discrepancy for differences higher than 25 per cent.

seems quite satisfactory. We would like to note here that (Hoshiba 1993) showed that the final result did not depend on the components used to perform the calculations. Main discrepancies happen in two stations: YAMAG2 in Yamagata prefecture and NIIGA2 in Niigata prefecture.

In Figs B1 and B2, we show the errors in the calculation of Q_s^{-1} and Q_i^{-1} . The errors have computed from the variance–covariance matrix for each fitting in each station. The maps do not show a

random distribution. The errors depend on the area and are probably related with the degree of heterogeneity in the crust of Japan. However, many different kinds of heterogeneities can be considered since the crust in Japan is very complex and many different processes, as the subduction of tectonic plates, volcanism and up flows from the dehydration of the tectonics plates takes place. Then it is difficult to establish what a degree of heterogeneity may indicate under such circumstances.

Table B3. Comparison with Hoshiba's results (1993) for frequency band 4–8 Hz.

Station name	Q_c^{-1} (1)	Q_c^{-1} (2)	Q_s^{-1} (1)	Q_s^{-1} (2)	Q_i^{-1} (1)	Q_i^{-1} (2)
KAGOS2	2.8	3.3	0.87(-0.51)	0.51	3.5(-0.9)	2.9
KUMAM2	2.6	3.2	0.48	0.55	2.5	2.5
SHIMO2	1.9	1.9	0.53	0.51	1.7	1.9
YONAG2	1.7	1.9	0.61	0.68	1.7	1.65
TOKUS2	2	2	0.19(+0.09)	0.35(-0.15)	1.7	1.75
WAKAY2	2.6	2.9	0.36(+0.12)	0.5(-0.15)	2.2	2.4
TSURU2	1.8	2.4	0.4(+0.23)	0.72(-0.23)	1.8	1.9
CHICH2	2	1.9	0.38(+0.39)	0.5	1.74	1.8
MATSU2	2.8	3	1.08(-0.46)	0.60	3.1(-0.8)	2.5
KAKIO2	2	2.3	0.95(-0.48)	0.61	2.2	2.2
NIIGA2	2	2.7	0.28(+0.13)	0.73(-0.22)	2.1	2.2
YAMAG2	1.7	2.5	0.29(+0.09)	0.65(-0.34)	1.5(+0.3)	2.2(-0.50)
OFUNA2	1.7	1.75	0.56	0.54	1.8	1.9
AOMOR2	2.1	2.7	0.64	0.55	2(+0.4)	2.45
HIROO2	1.8	2	0.59	0.57	1.85	2.1
KUSHI2	1.9	2	0.58(+0.37)	0.64	2.1	2.16

Notes: Hoshiba's results are indicated by (1) and ours by (2). Discrepancies are indicated by bold numbers. The criterion for discrepancy is that the result from Hoshiba does not match our result inside error bounds. We provide error bounds between brackets when necessary. For Q^{-1} we considered that there is a discrepancy for differences higher than 25 per cent.

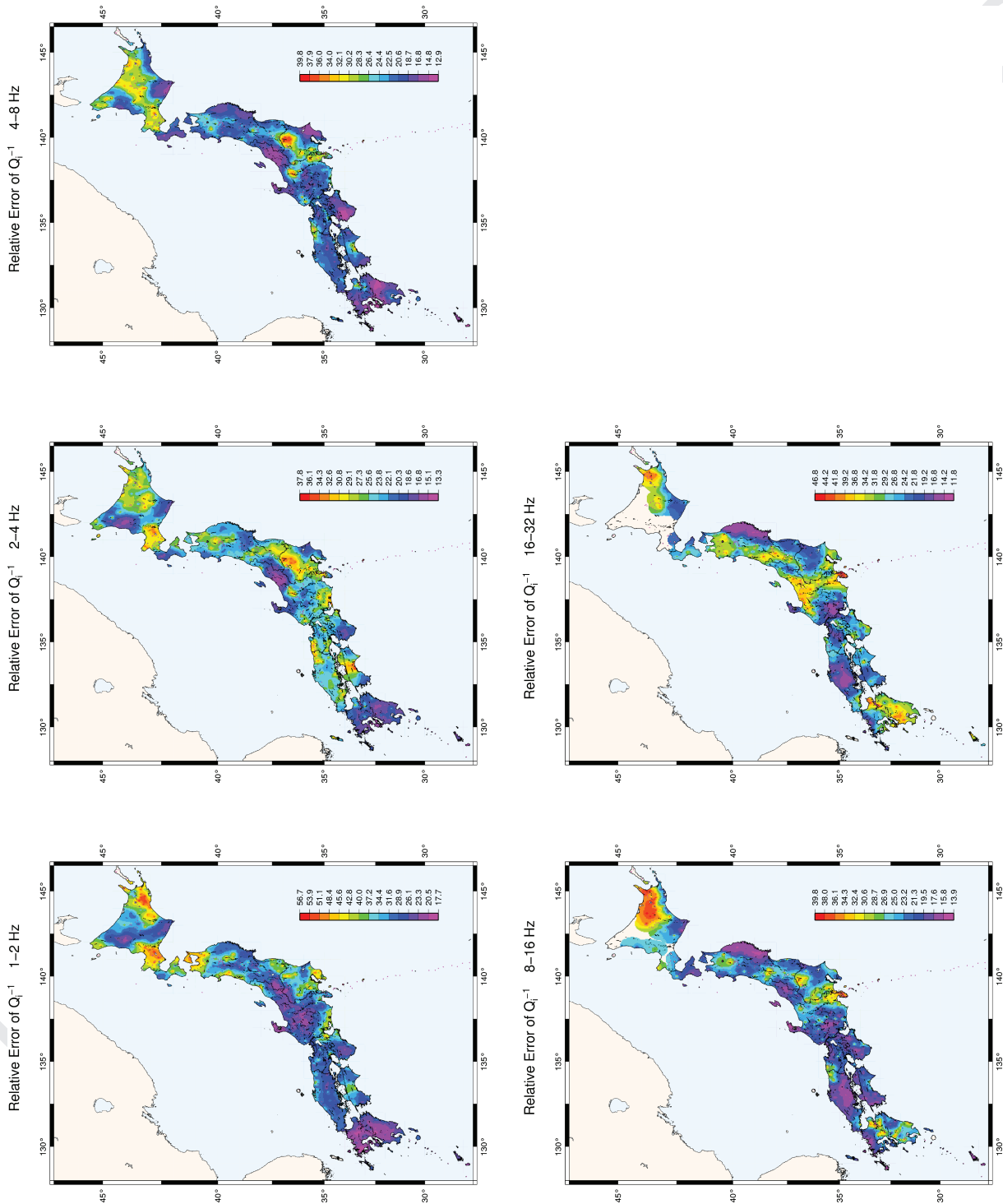


Figure B1. Estimation of the errors computed by using the variance-covariance matrix of each fitting for Q_1^{-1} for each frequency band.



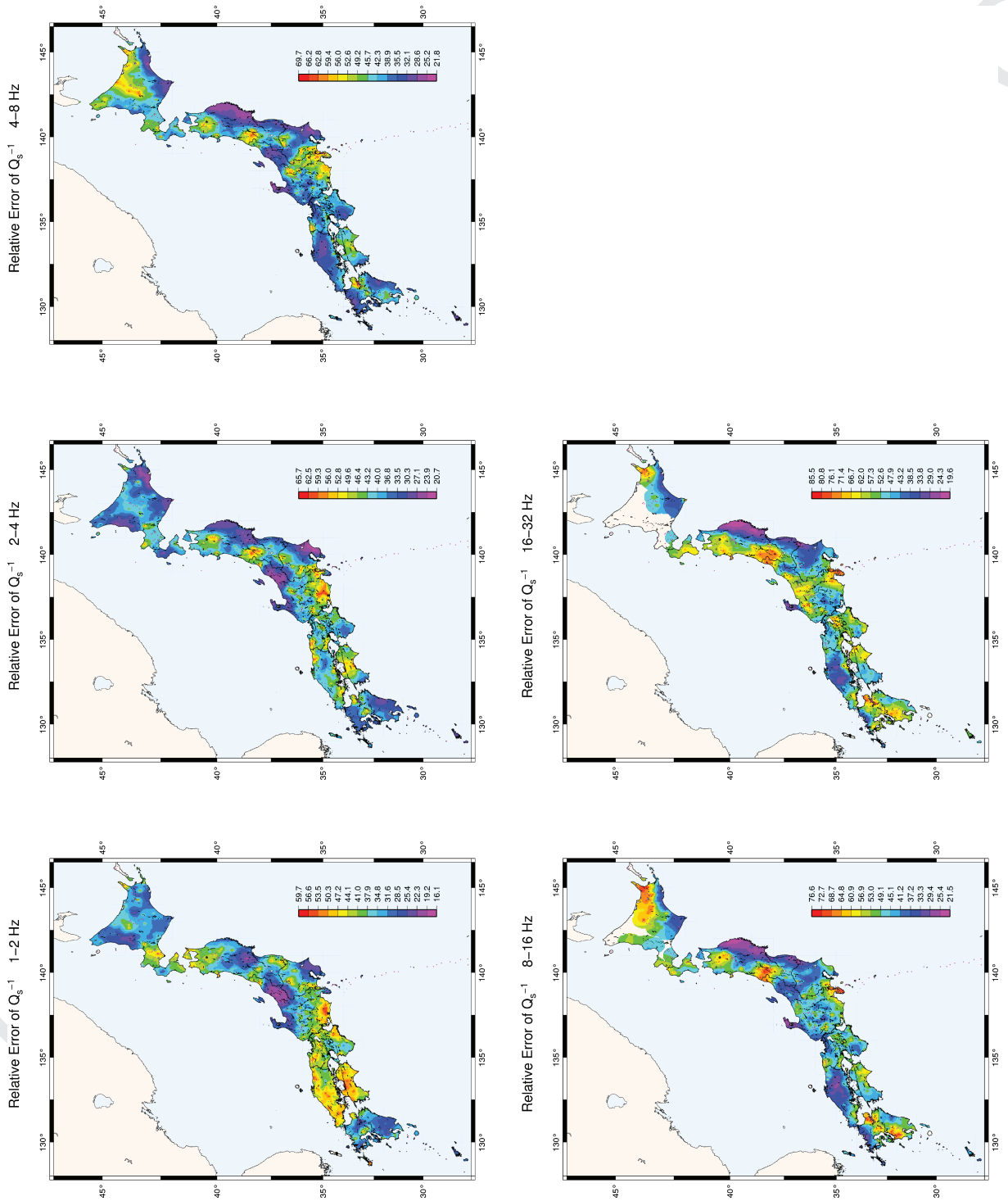


Figure B2. Estimation of the errors computed by using the variance-covariance matrix of each fitting for Q_s^{-1} for each frequency band.

1
2
3 **Queries**

4 Journal: GJI
5 Paper: gji_4394
6

7
8 Dear Author

9 During the copy-editing of your paper, the following queries arose. Please respond to these by marking up your proofs with
10 the necessary changes/additions. Please write your answers on the query sheet if there is insufficient space on the page proofs.
11 Please write clearly and follow the conventions shown on the corrections sheet. If returning the proof by fax do not write too
12 close to the paper's edge. Please remember that illegible mark-ups may delay publication.
13
14
15
16

Query Reference	Query	Remarks
Q1	Author: Please check and confirm that you are happy with the section to which this paper has been assigned: a list of all the sections can be found in the Author Guidelines (http://www.wiley.com/bw/submit.asp?ref=0956-540X&site=1).	
Q2	Author: As per journal style only a maximum of up to six keywords are allowed. Please check.	
Q3	>Author: A running head short title was not supplied; please check if this one is suitable and, if not, please supply a short title of up to 45 characters that can be used instead.	
Q4	Author: Reference Press <i>et al.</i> (2007) has not been included in the Reference List, please supply full publication details.	
Q5	>Author: Reference Sato & Fehler (1993) has not been included in the Reference List, please supply full publication details.	
Q6	Author: Reference Ueda <i>et al.</i> (2005) has been changed to Ueda (2005) to match the reference list. Please check.	
Q7	Author: Reference Jin & Aki (2002) has not been included in the Reference List, please supply full publication details.	
Q8	Author: If reference Aoyama <i>et al.</i> (2002) is not a one-page article please supply the first and last pages for this article.	
Q9	Author: Please list all authors if eight or fewer in reference Arita <i>et al.</i> (1998).	
Q10	>Author: Please list all authors if eight or fewer in reference Asano <i>et al.</i> (2004) and also provide page range or doi code for the same.	
Q11	Author: Please provide page range or doi code for reference Carcole <i>et al.</i> (2006).	
Q12	Author: Please list all authors if eight or fewer in reference Fehler <i>et al.</i> (1992).	

17
18
19
20
21
22
23
24
25
26
27
28
29
30
31
32
33
34
35
36
37
38
39
40
41
42
43
44
45
46
47
48
49
50
51
52
53
54
55
56
57
58
59
60
61
62
63
64

Q13	Author: Please list all the authors if eight or fewer for reference Hasegawa <i>et al.</i> (2005).	
Q14	>Author: Reference Lindquist <i>et al.</i> (2004) has not been cited in the text. Please indicate where it should be cited; or delete from the Reference List. If this is not a one-page article please supply the first and last pages for this article.	
Q15	Author: Please provide page range or doi code for reference Nakajima <i>et al.</i> (2007).	
Q16	>Author: Please list all the authors if eight or fewer for references Nakajima <i>et al.</i> (2001a,b).	
Q17	>Author: Please list all the authors if eight or fewer and also provide page range or doi code for reference Nakamura <i>et al.</i> (2006).	
Q18	Author: Please list all the authors if eight or fewer for reference Nakamura <i>et al.</i> (2008).	
Q19	>Author: Reference Nakata & Imaizumi (2002) has not been cited in the text. Please indicate where it should be cited; or delete from the Reference List.	
Q20	Author: If reference Mizoue <i>et al.</i> (1983) is not a one-page article please supply the first and last pages for this article.	
Q21	Author: Please provide page range or doi code for reference Obara <i>et al.</i> (2005).	
Q22	Author: Please list all the authors if eight or fewer for reference Sato <i>et al.</i> (2004).	
Q23	Author: Please list all the authors if eight or fewer for reference Takahashi <i>et al.</i> (2007).	
Q24	Author: Please list all the authors if eight or fewer for reference Tsumura <i>et al.</i> (2000).	
Q25	Author: Please provide page range or doi code for reference Ueda (2005).	
Q26	Author: Please list all the authors if eight or fewer and also provide publisher location for reference William <i>et al.</i> (2007).	
Q27	>Author: Please check the significance of italic values appearing in Tables B1–B3.	

Key words

Authors are requested to choose key words from the list below to describe their work. The key words will be printed underneath the summary and are useful for readers and researchers. Key words should be separated by a semi-colon and listed in the order that they appear in this list. An article should contain no more than six key words.

GEOPHYSICAL METHODS

Time series analysis
Image processing
Neural networks, fuzzy logic
Numerical solutions
Fourier analysis
Wavelet transform
Instability analysis
Inverse theory
Numerical approximations and analysis
Persistence, memory, correlations, clustering
Probabilistic forecasting
Spatial analysis
Downhole methods
Tomography
Interferometry
Thermobarometry
Fractals and multifractals
Non-linear differential equations
Probability distributions
Self-organization

GEODESY and GRAVITY

Satellite geodesy
Reference systems
Sea level change
Space geodetic surveys
Seismic cycle
Transient deformation
Gravity anomalies and Earth structure
Geopotential theory
Time variable gravity
Earth rotation variations
Global change from geodesy
Lunar and planetary geodesy and gravity
Radar interferometry
Plate motions
Tides and planetary waves
Acoustic-gravity waves

GEOMAGNETISM and ELECTROMAGNETISM

Electrical properties
Electromagnetic theory
Magnetotelluric
Non-linear electromagnetics
Archaeomagnetism
Biogenic magnetic minerals
Dynamo: theories and simulations
Environmental magnetism
Geomagnetic excursions
Geomagnetic induction
Magnetic anomalies: modelling and interpretation
Magnetic and electrical properties
Magnetic fabrics and anisotropy
Magnetic mineralogy and petrology
Magnetostratigraphy
Palaeointensity

Palaeomagnetic secular variation

Palaeomagnetism applied to tectonics

Palaeomagnetism applied to geologic processes

Rapid time variations

Remagnetization

Reversals: process, time scale, magnetostratigraphy

Rock and mineral magnetism

Satellite magnetics

Marine magnetics and palaeomagnetism

Marine electromagnetics

GENERAL SUBJECTS

Geomorphology

Geomechanics

Glaciology

Hydrogeophysics

Ionosphere/atmosphere interactions

Ionosphere/magnetosphere interactions

Gas and hydrate systems

Ocean drilling

Hydrology

Ultra-high pressure metamorphism

Ultra-high temperature metamorphism

Tsunamis

Thermochronology

Heat flow

Hydrothermal systems

Mantle processes

Core, outer core and inner core

COMPOSITION and PHYSICAL PROPERTIES

Microstructures

Permeability and porosity

Plasticity, diffusion, and creep

Composition of the core

Composition of the continental crust

Composition of the oceanic crust

Composition of the mantle

Composition of the planets

Creep and deformation

Defects

Elasticity and anelasticity

Equations of state

High-pressure behaviour

Fracture and flow

Friction

Fault zone rheology

Phase transitions

SEISMOLOGY

Controlled source seismology

Earthquake dynamics

Earthquake ground motions

Earthquake source observations

Seismic monitoring and test-ban

treaty verification

Palaeoseismology

Earthquake interaction, forecasting, and prediction

Seismicity and tectonics

Body waves

Surface waves and free oscillations

Interface waves

Guided waves

Coda waves

Seismic anisotropy

Seismic attenuation

Site effects

Seismic tomography

Volcano seismology

Computational seismology

Theoretical seismology

Statistical seismology

Wave scattering and diffraction

Wave propagation

Acoustic properties

Early warning

Rheology and friction of fault zones

TECTONOPHYSICS

Planetary tectonics

Mid-ocean ridge processes

Transform faults

Subduction zone processes

Intra-plate processes

Volcanic arc processes

Back-arc basin processes

Cratons

Continental margins: convergent

Continental margins: divergent

Continental margins: transform

Continental neotectonics

Continental tectonics: compressional

Continental tectonics: extensional

Continental tectonics: strike-slip and transform

Sedimentary basin processes

Oceanic hotspots and

intraplate volcanism

Oceanic plateaus and

microcontinents

Oceanic transform and fracture zone processes

Submarine landslides

Submarine tectonics and volcanism

Tectonics and landscape evolution

Tectonics and climatic interactions

Dynamics and mechanics of faulting

Dynamics of lithosphere and mantle

Dynamics: convection currents, and mantle plumes

Dynamics: gravity and tectonics

Dynamics: seismotectonics

Heat generation and transport

Impact phenomena

Hotspots

Large igneous provinces
Lithospheric flexure
Obduction tectonics
Neotectonics
Diapir and diapirism
Folds and folding
Fractures and faults
Kinematics of crustal and mantle deformation
High strain deformation zones
Crustal structure
Mechanics, theory, and modelling
Rheology: crust and lithosphere
Rheology: mantle

PLANETS

Planetary interiors
Planetary volcanism

VOLCANOLOGY

Physics of magma and magma bodies
Magma chamber processes
Magma genesis and partial melting
Pluton emplacement
Effusive volcanism
Mud volcanism
Subaqueous volcanism
Explosive volcanism
Volcaniclastic deposits
Volcano/climate interactions
Atmospheric effects (volcano)
Volcanic gases
Lava rheology and morphology
Magma migration and fragmentation
Eruption mechanisms and flow emplacement
Physics and chemistry of magma bodies

Calderas
Experimental volcanism
Tephrochronology
Remote sensing of volcanoes
Volcano monitoring
Volcanic hazards and risks

GEOGRAPHIC LOCATION

Africa
Antarctica
Arctic region
Asia
Atlantic Ocean
Australia
Europe
Indian Ocean
North America
Pacific Ocean
South America

MARKED PROOF

Please correct and return this set

Please use the proof correction marks shown below for all alterations and corrections. If you wish to return your proof by fax you should ensure that all amendments are written clearly in dark ink and are made well within the page margins.

<i>Instruction to printer</i>	<i>Textual mark</i>	<i>Marginal mark</i>
Leave unchanged	••• under matter to remain	Ⓧ
Insert in text the matter indicated in the margin	λ	New matter followed by λ or λ [Ⓧ]
Delete	/ through single character, rule or underline or ┌───┐ through all characters to be deleted	σ or σ [Ⓧ]
Substitute character or substitute part of one or more word(s)	/ through letter or ┌───┐ through characters	new character / or new characters /
Change to italics	— under matter to be changed	⎵
Change to capitals	≡ under matter to be changed	≡
Change to small capitals	== under matter to be changed	==
Change to bold type	~ under matter to be changed	~
Change to bold italic	≈ under matter to be changed	≈
Change to lower case	Encircle matter to be changed	≠
Change italic to upright type	(As above)	⊕
Change bold to non-bold type	(As above)	⊖
Insert 'superior' character	/ through character or λ where required	γ or γ ^λ under character e.g. γ ^λ or γ ^λ
Insert 'inferior' character	(As above)	λ over character e.g. λ
Insert full stop	(As above)	⊙
Insert comma	(As above)	,
Insert single quotation marks	(As above)	ʹ or ʸ and/or ʹ or ʸ
Insert double quotation marks	(As above)	“ or ” and/or “ or ”
Insert hyphen	(As above)	⎵
Start new paragraph	┌	┌
No new paragraph	~	~
Transpose	┌┐	┐┌
Close up	linking ○ characters	Ⓧ
Insert or substitute space between characters or words	/ through character or λ where required	Y
Reduce space between characters or words		↑